



The emplacement history of granitic intrusions into the upper crust: Forceful to passive emplacement of the early Miocene Solarya Pluton (NW Turkey) as a case study

Alp Ünal^{a,*}, Şafak Altunkaynak^a, Ömer Kamacı^a, Istvan Dunkl^b, Jeffrey A. Benowitz^c

^a Department of Geological Engineering, Istanbul Technical University, Maslak 34469, Istanbul, Turkey

^b Geoscience Center, University of Göttingen, Göttingen, Germany

^c Geophysical Institute, University of Alaska Fairbanks, PO Box 755940, Fairbanks, AK 99775, USA

ARTICLE INFO

Keywords:

Shallow intrusion
Pluton emplacement
Extension
NW Anatolia
Geothermo-barometry

ABSTRACT

Post-collisional magmatism in western Anatolia produced several granitic bodies represented by shallow level intrusions. In this study, we present field, geochronology and geothermo-barometry results of the Solarya Pluton (SP, NW Turkey) in order to better understand its emplacement into the different levels of the crust. The SP consists of three main plutonic members showing different textural properties; the northern part of the plutonic body is represented by K-feldspar megacrystalline granodiorite (KFMG) with distinct porphyritic texture and southern part is made up of microgranite-granodiorite (MGG) displaying microgranular texture whereas haplogranite, which displays graphic/granophyric textures, is represented by a thin aureole between the SP and basement rocks.

Field relations, petrography and geothermo-barometry studies combined with ⁴⁰Ar/³⁹Ar and U-Pb zircon dating results suggest that different members of the SP were emplaced into different levels of crust with different mechanisms. The KFMG (⁴⁰Ar/³⁹Ar – 23.2 Ma, U-Pb – 21.8 Ma) began its emplacement forcefully in the relatively deeper levels in the crust (av. 1.65 kbar; av. 797 °C; 6.1 km depth). After this stage, MGG (⁴⁰Ar/³⁹Ar – 22.6 Ma, U-Pb – 21.2 Ma) was passively emplaced into the shallow levels (av. 0.69 kbar; av. 745 °C; 2.4 km depth) via cauldron subsidence and in the latter stages the sheet intrusive rocks (haplogranite ⁴⁰Ar/³⁹Ar – 21.6 Ma and hypabyssal association) were emplaced into the ring faults at 1.5 km depth. Forceful to passive emplacement of the SP into the upper crust occurred under Aegean extensional tectonics. Our study contributes to examination of the granite ascent and emplacement within other extensional provinces worldwide.

1. Introduction

The emplacement of granites is defined as the switch of upward flow to the horizontal flow in the middle to upper crust, which started its ascent through the lower crust (Brown, 1994; Clemens, 1998; Marsh, 1982; Petford et al., 2000; Pitcher, 1979). The emplacement mechanisms of the plutons have been a popular matter of debate for the last century (e.g. Clough et al., 1909; Richey, 1928, 1932; Hutton, 1988; McCaffrey and Petford, 1997; Altunkaynak and Yilmaz, 1999; Petford et al., 2000, Cole et al., 2005; Stevenson et al., 2007, 2008; Stevenson, 2009). The main mechanisms that control the granite emplacement can be summarized as forceful emplacement, roof uplift, magmatic stopping and cauldron (floor) subsidence (e.g. Richey, 1928, 1932; Paterson and Fowler, 1993; Cruden, 1998; Petford, et al., 2000; Cole et al., 2005; Stevenson, 2009). From the early stages of the granite emplacement

research, the forceful emplacement mechanism has been controversial. The main point of this controversy is the so-called space problem (Pitcher, 1993) in which the forceful emplacement of magma occurs when the amount of magma exceeds the rate of the space therefore magma is required to shoulder aside the country rocks (Stevenson, 2009). Conversely pluton emplacement by floor subsidence through a cauldron subsidence mechanism, involves the sinking of a large block of country rock, controlled by the steep fractures or faults, into the magma chamber in which the space created by subsidence is filled by magma from the same magma chamber (Clough et al., 1909; Anderson, 1936; Hills, 1963; Hall, 1996; Cole et al., 2005; Stevenson et al., 2007; Stevenson, 2009).

In order to contribute to the debates on granite transport and emplacement space problems, we have undertaken the detailed field, geothermobarometry and geochronology studies in the Solarya Pluton

* Corresponding author.

E-mail address: alp.unal@itu.edu.tr (A. Ünal).

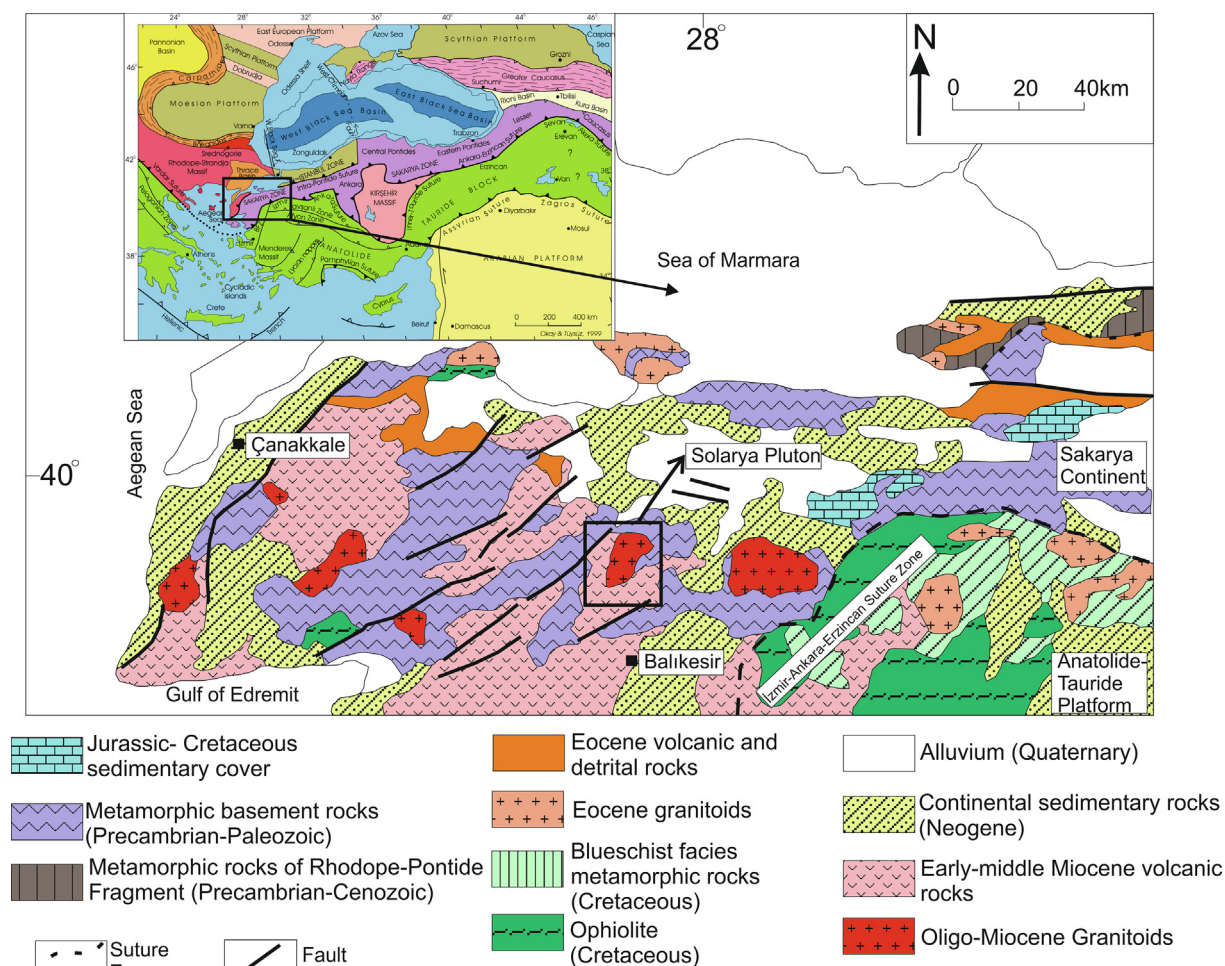


Fig. 1. Simplified geological map of the NW Anatolia (Modified from Altunkaynak, 2007). Black rectangle shows the Solarya Pluton (SP).

(SP), which is located at NW Anatolia within the western Anatolian extensional province (Fig. 1). The SP is one of the best examples of shallow level intrusions where the wall and roof rock relationships are clear and the indicators of different emplacement mechanisms are traceable. There are few studies in the literature which include geochemical and geochronological properties of the SP (Altunkaynak et al., 2012; Boztuğ et al., 2009; Çelebi and Köprübaşı, 2014; Karacık et al., 2008; Ünal and Altunkaynak, 2018; Yilmazer et al., 2014). However, the lack of integrated emplacement and cooling ages (U-Pb zircon and $^{40}\text{Ar}/^{39}\text{Ar}$ ages), emplacement conditions and emplacement mechanisms of the SP in the literature stand out in relief.

We present here geochronology (U-Pb zircon, $^{40}\text{Ar}/^{39}\text{Ar}$ biotite and feldspar) and amphibole-feldspar geothermo-barometry results of the different granitic members of the SP to examine the timing and conditions of the emplacement which occurred at different depths with different mechanisms. Contact relationships and structural data indicate that the emplacement of the SP has occurred with successive forceful emplacement and cauldron subsidence mechanisms. Regarding these multiple emplacement stages and emplacement mechanisms of the SP, this study contributes to examination of the journey of granitic magmas in the upper crust as well as the interplay between different emplacement stages and mechanisms.

2. Geological setting

2.1. Regional geology

Crustal structure of western Anatolia and broader Aegean

extensional province is made up of different continental blocks that were amalgamated via collision between Anatolide-Tauride platform and Sakarya Continent marked by the İzmir-Ankara-Erzincan Suture Zone (IAESZ) (Şengör and Yılmaz, 1981; Okay, 1984; Okay et al., 1990). In northwestern Anatolia, the basement units are Anatolide-Tauride platform (ATP), İzmir-Ankara-Erzincan Suture Zone (IAESZ), Sakarya Continent (SC), Intra-Pontide Suture Zone (IPSZ) and Rhodope Massif (RM), from south to north (Fig. 1). During the Late Oligocene-Early Miocene, a number of shallow level intrusions were emplaced into these different basement units following the continental collision. These shallow level intrusions are cogenetic and coeval with associated hypabyssal and volcanic rocks (Genç and Yılmaz, 1997; Altunkaynak and Dilek, 2006; Helvacı et al., 2009; Altunkaynak et al., 2010, 2012; Erkül, 2012; Kamacı and Altunkaynak, 2019a and b; Ünal and Altunkaynak, 2018). The SP, one of the representative examples of Early Miocene granitoids in NW Anatolia, was emplaced into the basement rocks of Sakarya Continent. Different rock groups are distinguished in the study area (Fig. 2). These are; (1) Basement rocks (metamorphic and non-metamorphic), (2) Solarya Pluton (SP), (3) Hypabyssal Association (HA), (4) Volcanic Association (VA) and (5) Sedimentary Association (SA).

2.2. Pluton interior

The SP is represented by N-S elongated plutonic body covering approximately 220 km². It has approximately 20 km length and 10 km width. The long axis of the pluton strikes N05E (N-S) and the short axis strikes N85W (W-E). The SP consists of three nearly coeval granitic

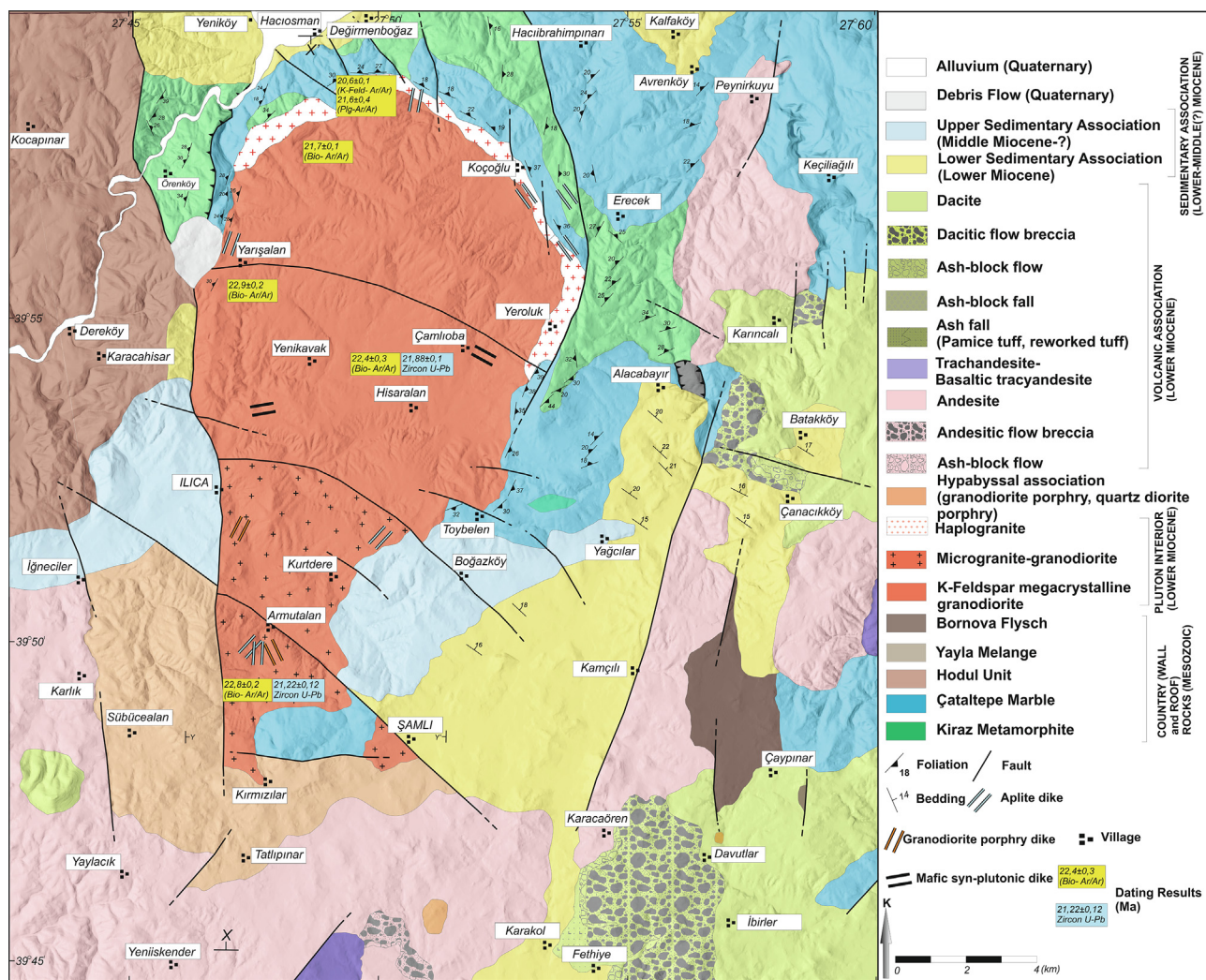


Fig. 2. Geological map of the study area (Modified after Ünal and Altunkaynak, 2018).

members (Fig. 2): (a) K-feldspar megacrystalline granodiorite (KFMG); (b) microgranite-granodiorite (MGG) and (c) haplogranite.

Northern part of the SP is formed from K-feldspar megacrystalline granodiorite (KFMG) whereas southern part is represented by microgranite-granodiorite (MGG). KFMG consists of plagioclase (oligoclase-andesine), quartz, K-feldspar (orthoclase), biotite and magnesio-hornblende. It presents holocrystalline porphyritic texture defined by K-feldspar megacrysts, reaching up to 5 cm size (Fig. 3a and b). Through the southern parts, the boundary between KFMG and MGG is bounded by a normal fault (Ilca Fault) striking 285° (W-E). MGG is characterized by its fine grained-microgranular texture (Fig. 3c and d). Along the southern contact of the pluton, MGG interfinger with porphyritic microgranodiorite/ microquartz-diorite (hypabyssal association, HA). Hypabyssal association (HA) is represented by crescent shaped sheet intrusive rocks presenting similar mineralogical properties with main plutonic body (Figs. 2 and 12a). They are typical with their microgranular, porphyritic texture. In some places, they include enclaves of MGG, and both HA and MGG are cut through by aplitic dikes.

Haplogranite is a fine-grained leucocratic-hololeucocratic variety of the main plutonic body and described by feldspar and quartz rich rocks with minor mafic minerals (biotite-amphibole < 5%). Graphic/granophytic textures are common in the haplogranites (for detailed petrographical properties of the SP, please see Ünal and Altunkaynak, 2018).

The SP is generally defined by a non-deformed isotropic granite. Only through the northern contacts of the pluton, a very narrow slight deformation zone was observed within KFMG. The marginal zone of the

pluton consists of semi-plastic reorientation of mica minerals and recrystallization of the quartz minerals. This deformation is mainly characterized by semi-ductile deformation possibly developed due to the emplacement of the pluton (Fig. 4). The present geomorphology of the pluton is mostly controlled by WNW-EES directed faults that cut different members of the SP. Ilca Fault, one of the major structural elements in the area, (marked as IF on Fig. 4) separates the K-Feldspar megacrystalline granodiorite (KFMG) and microgranite-granodiorite (MGG) and follows the primary contact between them. The Armutalan Fault (marked as AF on Fig. 4) is an active fault (Emre et al., 2018) and cuts the MGG together with basement and cover rocks.

2.3. Wall and roof rocks

The SP was intruded into the basement rocks of the Sakarya Continent which are represented by metamorphic (Nilüfer Unit) and non-metamorphic (Hodul Unit) rocks of Karakaya Complex (Okay et al., 1990). Nilüfer unit is represented by metabasites, metapelites and marbles (Okay et al., 1990). Metapelites are formed from quartz-mica schists, phyllites and calc-schists whereas metabasites are represented by metavolcanics and metatuffs (Fig. 5a and b). Marbles are mainly defined by dolomitic marbles (Fig. 5c and d).

The mineral assemblage in the metabasites is actinolite/hornblende + albite + chlorite + epidote whereas the intercalated mica-schists (metapelites) and calc-schists contain quartz + muscovite + biotite + chlorite ± garnet and

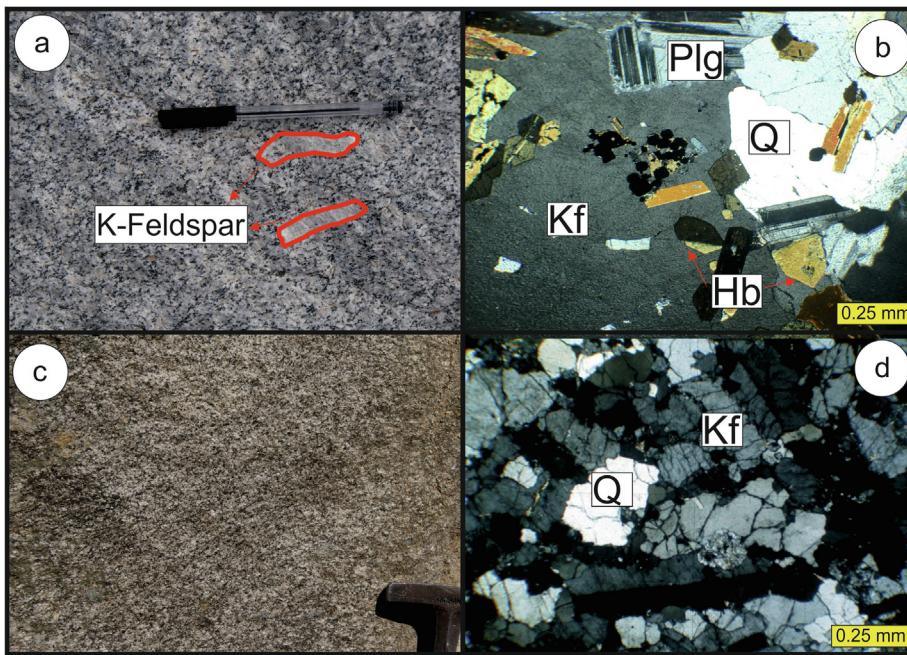


Fig. 3. (a) Field photograph of K-feldspar megacrystalline granodiorite (KFMG). (b) Micrograph illustrating the porphyritic texture of KFMG (Kf: K-Feldspar; Plg: Plagioclase; Q: Quartz; Hb: Hornblende). (c) Field photograph of microgranite-granodiorite (MGG). (d) Micrograph illustrating the microgranular texture of KFMG (Kf: K-Feldspar; Q: Quartz).

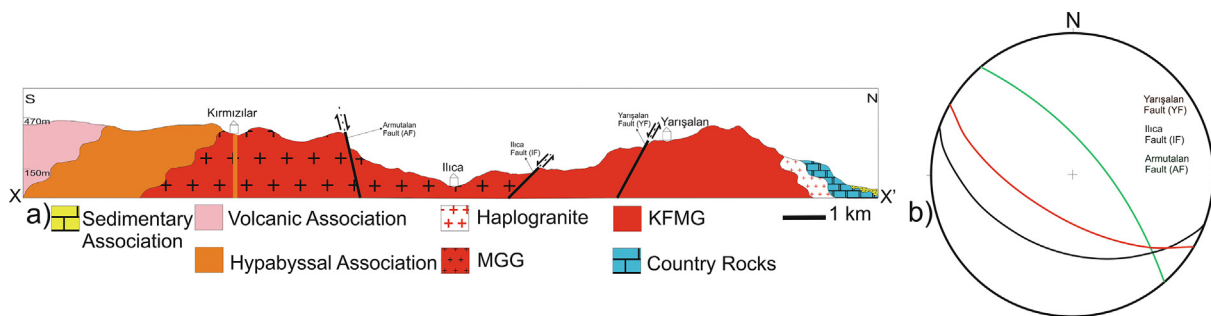


Fig. 4. (a) N-S cross-section of the study area (X-X'). Figure also illustrates the major faults cutting the SP. (b) Stereographic projection of three major faults.

quartz + muscovite + biotite + calcite, respectively (Fig. 5b). This mineral paragenesis indicate that, the metamorphism degree of Nilüfer Unit is within the limits of greenschist facies. They present well developed foliation (S-1) and lineation (L-1). The strike and dip directions of the foliation planes suggest that regional metamorphic rocks are represented by an anticline and its main fold axis strike through NE-SW (Fig. 2).

During the emplacement of the SP, a contact metamorphic aureole was developed between the SP and wall rocks mostly forming from dolomitic marbles and calc-schists. Mineralogical and structural changes developed by contact metamorphism can be observed through the northern and eastern contacts of the pluton with the wall rocks. Through the other contacts, the contact metamorphic zone is truncated by faults. The contact metamorphic rocks are represented by different lithologies. Through the contacts of the SP with dolomitic marbles, contact metamorphic rocks are formed from hornfels and skarn whereas along the contacts with calc-schists, contact metamorphic rocks are made up of contact schists. Hornfels and skarn display hornfels texture while contact schists display schistose texture defined by the slight elongation of the diopside and wollastonite with sub-grain rotations in quartz through a secondary developed foliation (S-2; Fig. 6a and b). The shear senses of the contact schists are perpendicular to the strike of the pluton contacts (Fig. 6a and b) whereas regional metamorphic rocks display complex shear senses. One of the other textural variation that is observed due to the contact metamorphism is the increasing grain size in marbles towards to the pluton boundary (Fig. 6c and d).

Contact metamorphic zone can be divided into two different zones (inner and outer) based on mineral paragenesis of contact metamorphic calc-schists. Inner zone is represented by wollastonite + diopside + hypersthene + plagioclase + garnet + quartz (Fig. 7 a, b and c). Outer zone, on the other hand, is located further from the main plutonic body and represented by calcite + plagioclase + tremolite + diopside + garnet + quartz + epidote (Fig. 7d-f). These mineral parageneses indicate that the conditions of contact metamorphism were reached to the pyroxene-hornfels facies for the inner zone, and hornblende-hornfels to epidote-hornfels facieses for the outer zone (Yardley et al., 1990).

The structural changes within the wall rocks through the eastern and northern contacts are not only characterized by micro scale variations, but also meso-macro scale structural features. At a distance from the pluton boundary, the trends of the foliation planes of the basement rocks are represented by an anticline and its representative fold axis strike through NE-SW (Fig. 8a and b). Closer to the contacts of the pluton, these trends progressively swing towards the contact, finally becoming concordant to the boundary (Fig. 8a and c).

Along the western border, contact metamorphic zone is truncated by a fault zone which separates the SP from the wall rocks (Fig. 2). The N-S trending normal fault with approximately 25 km length cuts two different main units (KFMG, MGG) of the pluton together with the country rocks. Through the fault zone, the pluton presents cataclastic textures in local places, indicating its brittle deformation. Therefore, this fault should have been active while the pluton is relatively cooled

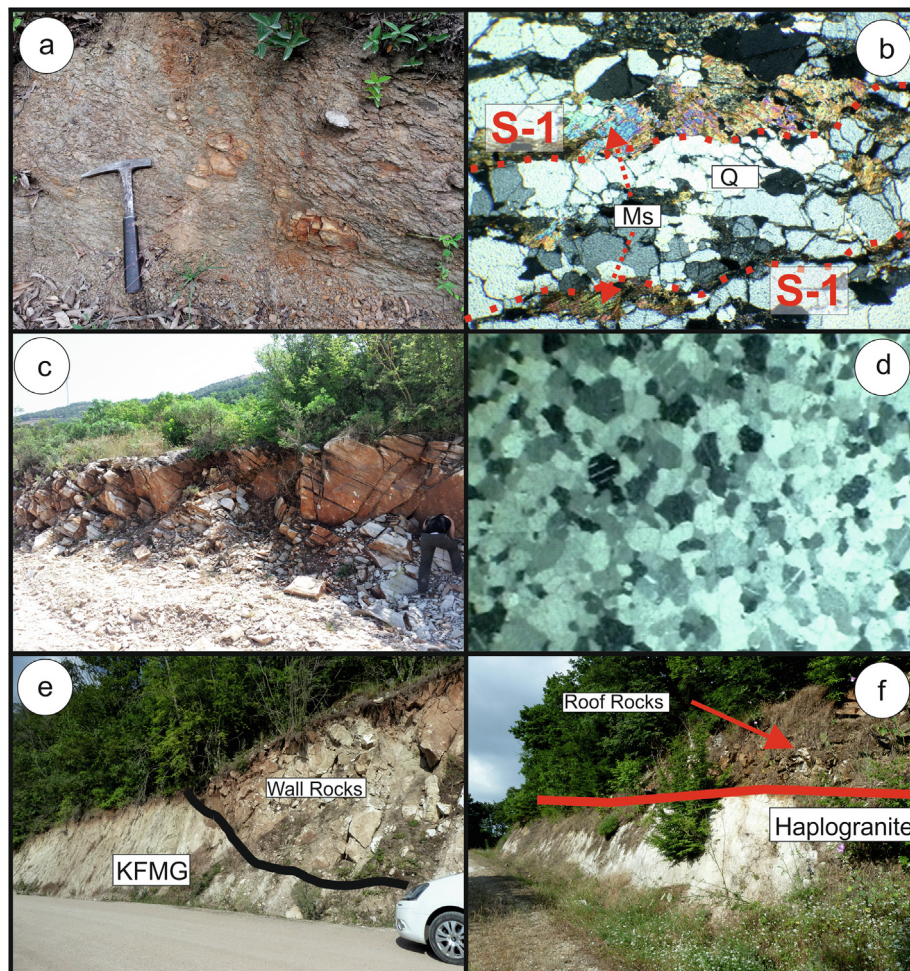


Fig. 5. (a) Field photograph of metapelites. (b) Micrograph of metapelites. The S-1 foliation plane is shown in the figure. (c) Field photograph of marbles. (d) Micrograph of marbles. (e) The contact intrusive between KFMG and wall rocks. (f) The contact between haplogranite and roof rocks.

down. Moreover, this N-S trending fault also cuts the upper sedimentary association in several places which overlays the plutonic body and presents younger ages than middle Miocene. These data indicate that, western contact of the pluton with country rocks is bounded by a relatively young, brittle fault. This young fault tucks away the haplogranite and contact metamorphic aureole through the western margin of the pluton.

Roof rocks are observed at the southern margin between the MGG and HA. The contacts between the MGG and roof rocks are smooth and gently dipping which are defined by the contacts with $< 10^\circ$ dip angles. In this place, the marbles represent a “roof pendant”, which is defined by the remnants of the roof rocks at the top of the pluton (Fig. 2).

2.4. Cover rocks

Cover rocks in the study area are represented by volcanic and sedimentary associations.

Volcanic Association (VA) covers an area of approximately 240 km² (Fig. 2) at the southern and eastern parts of the study area. It is formed from three main rock groups; (1) Andesite and associated pyroclastic rocks, (2) Dacite and related pyroclastic rocks (Fig. 9a), and (3) trachyandesite and dykes. Pyroclastic rocks are represented by flow breccias, pyroclastic fall and flow units (Ünal and Altunkaynak, 2019). Volcanic Association (VA) interfinger with hypabyssal association through southerly parts of the study area.

Sedimentary association can be divided into two different groups

based on their structural and lithological properties; (1) Lower Sedimentary Association (LSA) and (2) Upper Sedimentary Association (USA). LSA is formed from sequence of lacustrine sediments. It begins with a coarse-grained basal conglomerate which consists of pebbles of plutonic and basement rocks at the base. The upper parts of the conglomerate are defined by coarse-grained sandstones. A thick sequence of mudstone and shale with thin beddings overlays the sandstones through the northern parts. Shale and mudstones include thin lignite layers (Fig. 9b). The uppermost parts of LSA are formed from volcanoclastic rocks including reworked tuffs and conglomerate with volcanic pebbles. LSA interfingers with volcanic rocks in many places, however, the stratigraphically upper parts of the sequence penecontemporaneously overlays volcanic rocks as well. This relationship between the volcanic and sedimentary rocks suggests that both VA and LSA are coeval. Therefore, LSA presents lower to middle Miocene age.

USA consists of unlithified terrigenous sediments represented by coarse sand and pebble layers which were originated from different lithologies. There is no paleontological data from the upper sedimentary association neither in this study nor in the previous studies. However, since the upper sedimentary association overlays all units (except Quaternary units) in the area, it must be younger than middle Miocene time. USA consists of granodiorite blocks and pebbles (Fig. 9c and d) indicating that the SP was uplifted and exhumed before the deposition of the USA.

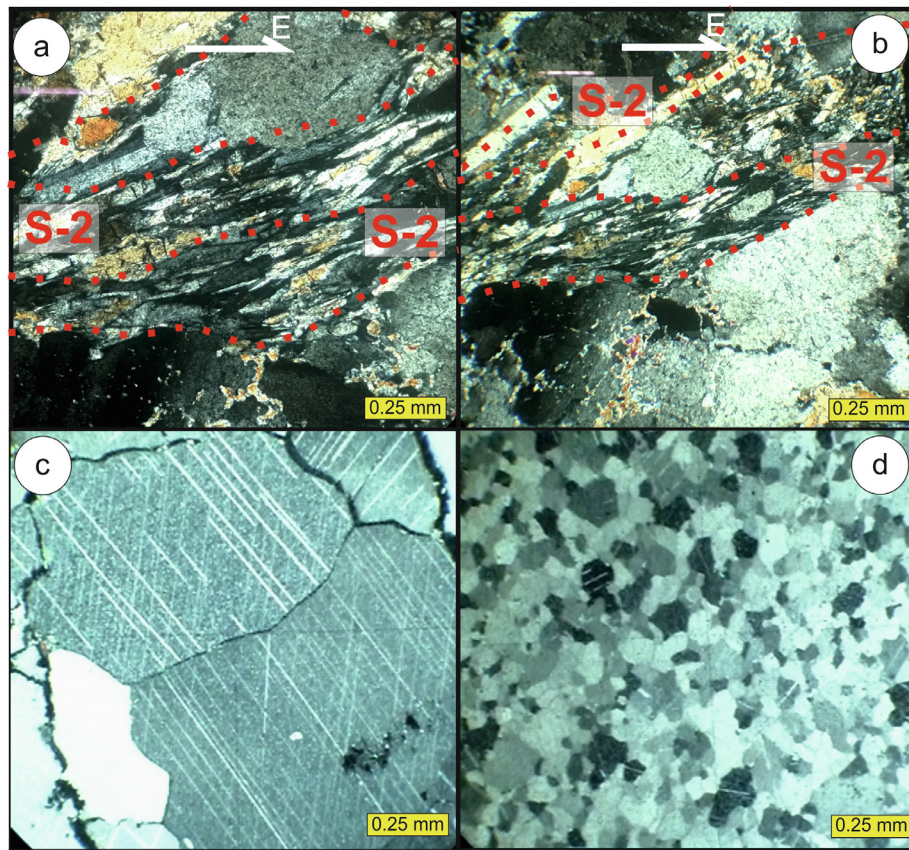


Fig. 6. (a, b) The elongation of wollastonite and diopside in contact schists over a secondary foliation plane (S-2). (c, d) Decrease of grain size in marbles outwards the pluton boundary.

3. Analytical methods

3.1. Geochronology

Zircon crystals were fixed on a double-side adhesive tape stuck on a thick glass plate and embedded in a 25 mm diameter epoxy mount. The crystal mounts were lapped by 2500 mesh SiC paper and polished by 9, 3 and 1 μm diamond suspensions.

For all zircon samples and standards used in this study cathodoluminescence (CL) images were obtained using a JEOL JXA 8900 electron microprobe at the Geozentrum Göttingen (Germany) in order to study their internal structure and to select homogeneous parts for the in-situ age determinations. The carbon coating used for CL imaging were later removed with a brief hand polish on a 1 micron diamond cloth. The mounts were cleaned in different steps with diluted HCl, ethanol and deionised water in an ultrasonic bath to remove surface lead contamination before introduction into the sample cell.

The in-situ U-Pb dating was performed by laser-ablation single-collector sector-field inductively coupled plasma mass spectrometry (LA-SF-ICP-MS). The method employed for analysis is described in details by Frei and Gerdes (2009). A Thermo Finnigan Element 2 mass spectrometer coupled to a Resonetics Excimer laser ablation system was used. All age data presented here were obtained by single spot analyses with a laser beam diameter of 33 μm and a crater depth of approximately 10 μm . The laser was fired at a repetition rate of 5 Hz and at nominal laser energy output of 25%. Two laser pulses were used for pre-ablation. The carrier gas was He and Ar. Analytes of ^{238}U , ^{235}U , ^{232}Th , ^{208}Pb , ^{207}Pb , ^{206}Pb , mass 204 and ^{202}Hg were measured by the ICP-MS. The data reduction is based on the processing of ca. 100 selected time slices (corresponding ca. 10.5 s) starting ca. 1 sec. after the beginning of the signal. If the ablation hit zones or inclusions with highly variable

actinide concentrations or isotope ratios then the integration interval was slightly resized or the analysis was discarded (~1% of the spots). The individual time slices were tested for possible outliers by an iterative Grubbs test (applied at $P = 5\%$ level). This test filtered out only the extremely biased time slices, and in this way usually less than 2% of the time slices were rejected. The age calculation and quality control are based on the drift- and fractionation-correction by standard-sample bracketing using GJ-1 zircon reference material (Jackson et al., 2004). For further control the Plešovice zircon (Sláma et al., 2008), the 91500 zircon (Wiedenbeck et al., 1995) and the FC-1 zircon (Paces and Miller, 1993) were analyzed as “secondary standards”. The age results of the standards were consistently within 2σ of the published ID-TIMS values. Drift- and fractionation-corrections and data reductions were performed by in-house software (UranOS; Dunkl et al., 2008). The level of Hg-corrected ^{204}Pb signal was very low, thus no common lead correction was required. The number of single-grain measurements per sample ranges between 24 and 29. The concordia plots and age spectra were constructed by the help of Isoplot/Ex 3.0 (Ludwig, 2003) and AgeDisplay (Sircombe and Hazelton, 2004).

For $^{40}\text{Ar}/^{39}\text{Ar}$ analysis, rock samples were submitted to the Geochronology laboratory at University of Alaska Fairbanks where it was crushed, sieved, washed and hand-picked for feldspar and biotite mineral phases. The monitor mineral MMhb-1 (Samson and Alexander, 1987) with an age of 523.5 Ma (Renne et al., 1994) was used to monitor neutron flux (and to calculate the irradiation parameter, J). The samples and standards were wrapped in aluminum foil and loaded into aluminum cans of 2.5 cm diameter and 6 cm height. The samples were irradiated in position 8b of the uranium enriched research reactor of McMaster University in Hamilton, Ontario, Canada for 150 megawatt-hours.

Upon their return from the reactor, the sample and monitors were

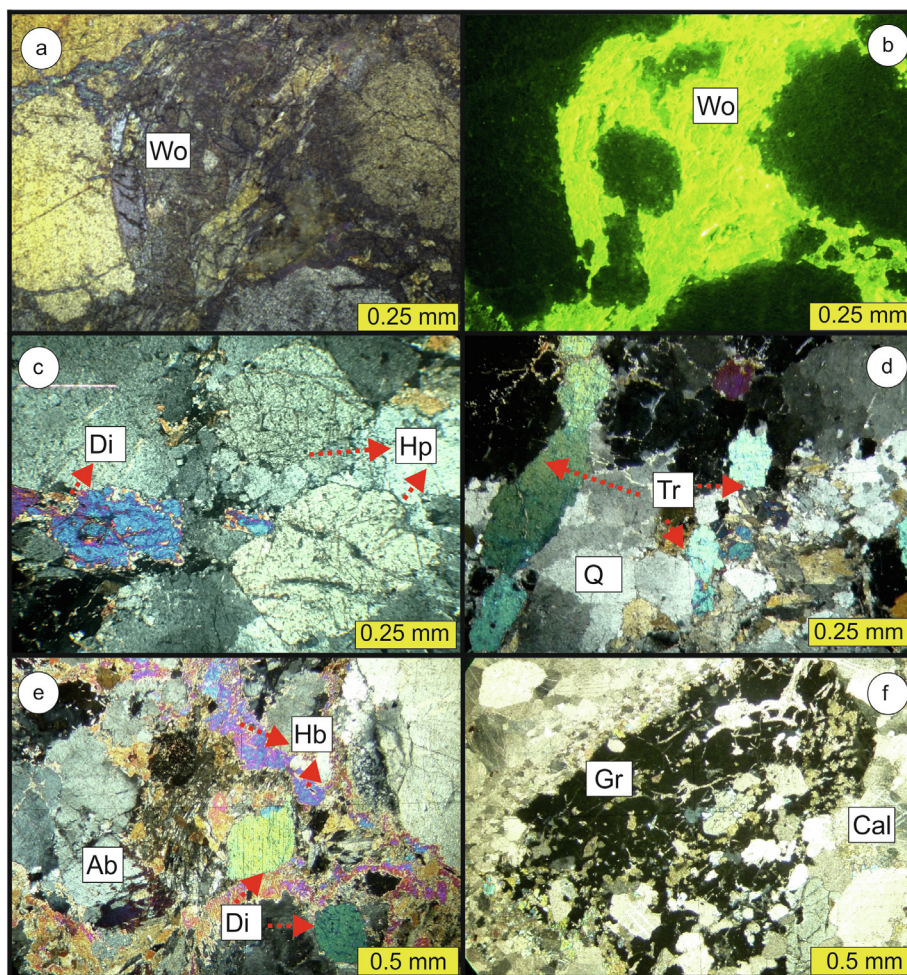


Fig. 7. Micrographs illustrating the main petrographical features of the contact metamorphic rocks. (a) Wollastonite (Wo) porphyroblast in hornfels near the contact. (b) Cathodoluminescence image of wollastonite (Wo) within the inner zone. (c) Co-existence of diopside (Di) and hyperstene (Hp) in the contact metamorphic rocks of the inner zone. (d) Tremolite (Tr) and quartz (Q) development in the contact metamorphic rocks towards the outer zone. (e) Hornblende (Hb), albite (Ab) and diopside (Di) paragenesis in the outer zone. (f) Garnet (Gr) with calcite (Cal) in the contact metamorphic rocks of the outer zone.

loaded into 2 mm diameter holes in a copper tray that was then loaded in an ultra-high vacuum extraction line. The monitors were fused, and samples heated, using a 6-watt argon-ion laser following the technique described in [Layer et al. \(1987\)](#) and [Benowitz et al. \(2014\)](#). Argon purification was achieved using a liquid nitrogen cold trap and a SAES Zr-Al getter at 400 °C. The samples were analyzed in a VG-3600 mass spectrometer at the Geophysical Institute, University of Alaska Fairbanks. The argon isotopes measured were corrected for system blank and mass discrimination, as well as calcium, potassium and chlorine interference reactions following procedures outlined in [McDougall et al. \(1999\)](#). Typical full-system 8 min laser blank values (in moles) were generally 2×10^{-16} mol ^{40}Ar , 3×10^{218} mol ^{39}Ar , 9×10^{-18} mol ^{38}Ar and 2×10^{-18} mol ^{36}Ar , which are 10–50 times smaller than the sample/standard volume fractions. Correction factors for nucleogenic interferences during irradiation were determined from irradiated CaF_2 and K_2SO_4 as follows: $(^{39}\text{Ar}/^{37}\text{Ar}) \text{Ca} = 7.06 \times 10^{-4}$, $(^{36}\text{Ar}/^{37}\text{Ar}) \text{Ca} = 2.79 \times 10^{-4}$ and $(^{40}\text{Ar}/^{39}\text{Ar}) \text{K} = 0.0297$. Mass discrimination was monitored by running calibrated air shots. The mass discrimination during these experiments was 0.8% per mass unit. While doing our experiments, calibration measurements were made on a weekly-monthly basis to check for changes in mass discrimination. No significant variation seen during these intervals.

A summary of $^{40}\text{Ar}/^{39}\text{Ar}$ results is given in [Table 1](#), with all ages quoted to the ± 1 sigma level and calculated using the constants of [Renne et al. \(2010\)](#). The integrated age is the age given by the total gas

measured and is equivalent to a potassium-argon (K-Ar) age. The spectrum provides a plateau age if three or more consecutive gas fractions represent at least 50% of the total gas release and are within two standard deviations of each other (Mean Square Weighted Deviation less than 2.5).

3.2. Mineral chemistry

Samples were analyzed at the University of Georgia Department of Geology with JEOL 8600 electron microprobe using a 15 KV accelerating voltage and 15 nA beam current. Minerals were qualitatively identified using a Bruker 5010 Silicon Drift Detector (SDD) energy dispersive X-ray (EDS) detector controlled by a Bruker Quantax energy dispersive analysis system. Quantitative analyses were performed with wavelength dispersive spectrometers (WDS) automated with Advanced Microbeam, Inc. electronics and Probe for EPMA software, using 10 s counting times, and natural and synthetic mineral standards. Analyses were calculated using [Armstrong and Clark \(1988\)](#) Phi-Rho-Z matrix correction model.

4. Results

4.1. U-Pb zircon chronology

U-Pb zircon dating method has been applied to two different

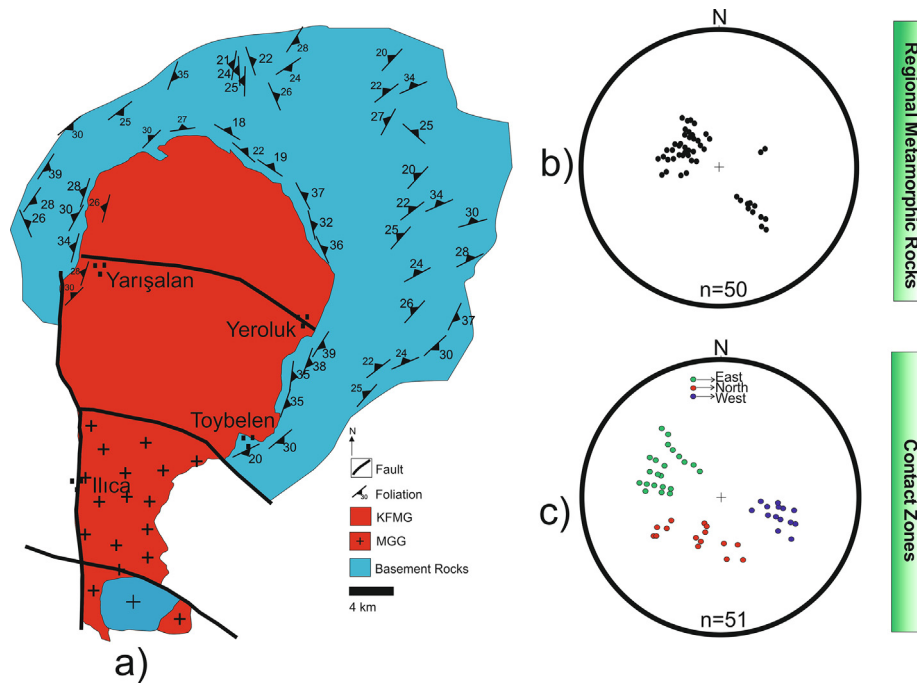


Fig. 8. (a) The structural geology map of the SP and surrounding rocks (wall rocks). (b) Steographic projections of the foliation planes of regional metamorphic rocks. (c) Steographic projections of the foliation planes of regional metamorphic rocks along the contact with the SP.

samples from the SP (one sample from K-Feldspar megacrystalline granodiorite (AS 211) and one sample from microgranite-granodiorite (AS 240)). Zircons from the host granite are prismatic and transparent with well-developed oscillatory zoning which indicates a magmatic origin. Their aspect ratio ranges between 1:2 and 1:3.5 (Fig. 10). Analyzed zircons present Th/U values between 0.52 and 1.06, consistent with a magmatic origin. From AS 211, twenty-nine spots were obtained and it presents a concordia age of 21.8 ± 0.2 Ma. From the other sample, AS 240, twenty-four spot analyses yielded concordia age of 21.2 ± 0.1 Ma (Fig. 10 and Table 2). These two consistent ages are considered to be the emplacement age of the SP.

4.2. $^{40}\text{Ar}/^{39}\text{Ar}$ biotite and feldspar chronology

The $^{40}\text{Ar}/^{39}\text{Ar}$ ages of the SP (three samples from KFMG, one from MGG and one from haplogranite) were obtained from biotite, K-feldspar and plagioclase separates. The ages are given in Table 2 and the isochron plots are shown in Fig. 11. All the samples produced generally flat age spectrum reflective of extremely rapid post emplacement cooling.

The five biotite separates display isochron ages between 21.8 ± 0.1 Ma and 23.2 ± 0.2 Ma whereas the K-feldspar and plagioclase separates yield plateau ages of 20.3 ± 0.2 Ma and

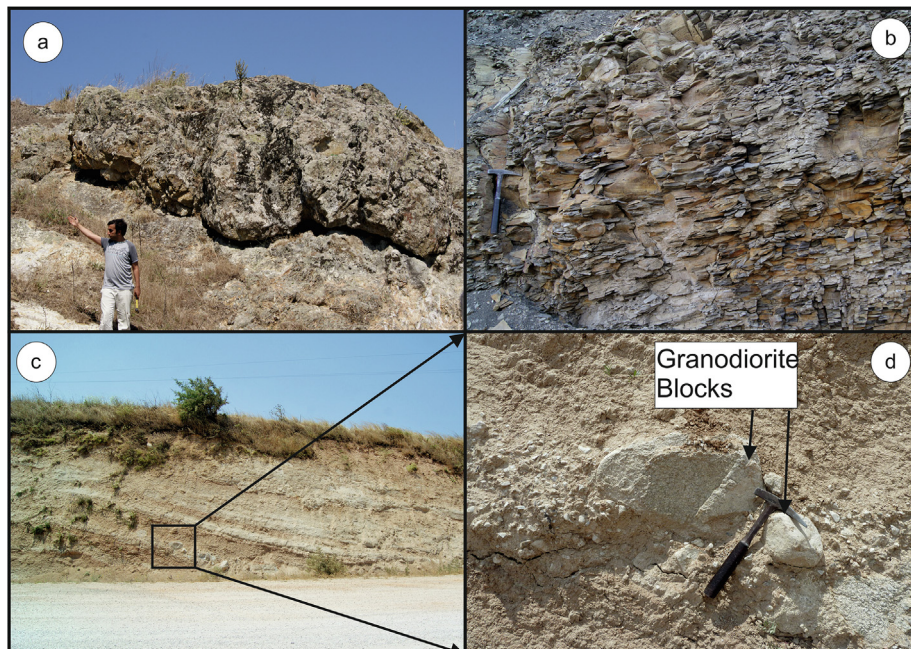


Fig. 9. Field photographs of volcanic and sedimentary association. (a) Dacite. (b) Sandstone of lower sedimentary association. (c) and (d) Upper sedimentary association with granodiorite blocks.

Table 1
Zircon U-Pb isotopic data for the SP.

Sample	Grain	U [ppm]	Pb [ppm]	Th U	²⁰⁶ Pb ²³⁸ U	± 1σ [%]	²⁰⁷ Pb ²³⁵ U	± 1σ [%]	²⁰⁷ Pb ²⁰⁶ Pb	± 1σ [%]	rho	²⁰⁶ Pb ²³⁸ U	± 2σ [Ma]	²⁰⁷ Pb ²³⁵ U	± 2σ [Ma]	²⁰⁷ Pb ²⁰⁶ Pb	± 2σ [Ma]	Disc. I. [%]
AS-211	6	713	352	0.589	0.003369	1.9	0.022408	8.7	0.04824	8.5	0.21	21.7	0.8	22.5	3.9	110.9	201.5	3.6
	7	832	429	0.617	0.00337	1.6	0.023213	5.7	0.04996	5.5	0.28	21.7	0.7	23.3	2.6	193.2	127.3	6.9
	8	872	539	0.729	0.003455	1.8	0.024506	4.7	0.05145	4.3	0.38	22.2	0.8	24.6	2.3	261.1	99.8	9.6
	9	620	316	0.609	0.003396	1.8	0.025029	6.2	0.05345	6	0.29	21.9	0.8	25.1	3.1	348	135.3	12.9
	10	609	280	0.549	0.003432	1.6	0.024574	5.3	0.05193	5	0.31	22.1	0.7	24.7	2.6	282.4	115.5	10.4
	11	780	375	0.575	0.003367	1.5	0.023581	6.4	0.0508	6.2	0.24	21.7	0.7	23.7	3	231.7	144.2	8.4
	12	1028	543	0.631	0.003352	1.6	0.023255	5.3	0.05032	5	0.3	21.6	0.7	23.3	2.4	209.9	116.4	7.6
	13	791	438	0.663	0.003304	1.8	0.024587	5.4	0.05397	5.1	0.34	21.3	0.8	24.7	2.6	369.7	114.7	13.8
	14	952	583	0.731	0.003442	1.8	0.022855	5.5	0.04816	5.2	0.33	22.1	0.8	22.9	2.5	107.4	123.5	3.5
	20	932	512	0.656	0.003403	1.2	0.02268	5.7	0.04834	5.6	0.21	21.9	0.5	22.8	2.6	116.2	131.4	3.8
	21	842	468	0.663	0.003306	1.5	0.027744	5.5	0.06087	5.3	0.27	21.3	0.6	27.8	3	634.6	115	23.4
	22	863	489	0.677	0.003425	1.5	0.026252	5.4	0.0556	5.2	0.27	22.0	0.6	26.3	2.8	436.3	115.1	16.2
	23	840	409	0.584	0.003801	2.0	0.042144	4.9	0.08042	4.4	0.41	24.5	1	41.9	4	1207.4	87.3	41.7
	24	952	496	0.621	0.003367	1.7	0.021931	4.5	0.04724	4.2	0.37	21.7	0.7	22	2	61.6	100.5	1.6
	25	1044	637	0.729	0.003449	1.5	0.022967	5.1	0.0483	4.9	0.3	22.2	0.7	23.1	2.3	114.1	114.7	3.7
	26	807	468	0.692	0.003399	1.9	0.021581	5.8	0.04604	5.5	0.32	21.9	0.8	21.7	2.5	0.1	47.3	-0.9
	27	1008	504	0.596	0.003433	1.8	0.022662	6.4	0.04788	6.2	0.28	22.1	0.8	22.8	2.9	93.5	146.6	2.9
	28	860	464	0.644	0.003426	1.8	0.022303	5	0.04721	4.6	0.36	22.1	0.8	22.4	2.2	59.9	109.9	1.6
	29	828	449	0.648	0.003367	1.8	0.023586	6.6	0.05081	6.4	0.27	21.7	0.8	23.7	3.1	232.1	146.8	8.5
	35	949	537	0.675	0.003433	1.7	0.022806	5.8	0.04819	5.6	0.3	22.1	0.8	22.9	2.6	108.6	131.4	3.5
	36	741	392	0.633	0.003279	1.7	0.024212	6.1	0.05356	5.9	0.28	21.1	0.7	24.3	2.9	352.7	133	13.1
	37	933	525	0.671	0.003314	1.7	0.02328	4.9	0.05095	4.6	0.35	21.3	0.7	23.4	2.3	238.4	107.2	8.7
	38	755	329	0.521	0.003319	1.7	0.022117	5.1	0.04834	4.8	0.34	21.4	0.7	22.2	2.2	115.9	112.3	3.9
	39	699	337	0.577	0.003582	1.9	0.030089	7.1	0.06092	6.8	0.26	23.1	0.9	30.1	4.2	636.3	146.8	23.4
	40	902	544	0.718	0.003283	1.9	0.021228	6.5	0.0469	6.2	0.29	21.1	0.8	21.3	2.8	44.2	149	0.9
	41	891	581	0.78	0.003466	1.9	0.022448	4.6	0.04698	4.1	0.42	22.3	0.9	22.5	2	48.2	98.9	1.1
	42	842	473	0.671	0.003468	1.7	0.029363	4.8	0.0614	4.5	0.34	22.3	0.7	29.4	2.8	653.5	96.7	24
	43	816	407	0.596	0.003356	1.8	0.021843	6.3	0.04721	6	0.28	21.6	0.8	21.9	2.7	60	143.1	1.6
	44	987	498	0.603	0.003436	1.5	0.022247	5.6	0.04696	5.4	0.27	22.1	0.7	22.3	2.5	47.1	129	1
AS-240	50	983	571	0.694	0.003238	1.6	0.021645	5.5	0.04848	5.3	0.28	20.8	0.7	21.7	2.4	123	124.6	4.2
	51	834	403	0.578	0.003242	1.6	0.0226	5.1	0.05056	4.9	0.32	20.9	0.7	22.7	2.3	221	112.7	8.1
	52	823	470	0.682	0.003338	1.7	0.027722	5.1	0.06023	4.8	0.34	21.5	0.7	27.8	2.8	611.8	102.8	22.6
	53	1059	634	0.713	0.003363	1.6	0.026838	4.6	0.05788	4.3	0.36	21.6	0.7	26.9	2.4	525.3	93.8	19.5
	54	673	338	0.597	0.003251	1.8	0.024983	5.9	0.05574	5.6	0.31	20.9	0.7	25.1	2.9	442.1	124.2	16.5
	55	777	377	0.581	0.003346	1.7	0.022301	6.8	0.04833	6.5	0.26	21.5	0.8	22.4	3	115.7	154.3	3.8
	56	743	390	0.628	0.003308	1.7	0.021417	6.2	0.04696	6	0.28	21.3	0.7	21.5	2.7	47.3	142.9	1.1
	57	1001	558	0.666	0.003355	1.8	0.024165	6.1	0.05223	5.8	0.29	21.6	0.8	24.2	2.9	295.7	132.1	10.9
	58	1254	783	0.746	0.0033	1.8	0.022107	5.5	0.04859	5.1	0.33	21.2	0.8	22.2	2.4	128.1	121.2	4.3
	59	687	349	0.608	0.004238	2.2	0.037398	5.4	0.064	4.9	0.41	27.3	1.2	37.3	3.9	741.8	103.9	26.9
	65	849	476	0.669	0.003426	1.8	0.028448	7.1	0.06023	6.9	0.25	22.0	0.8	28.5	4	612	148.7	22.6
	66	735	324	0.529	0.003318	2.0	0.021575	6.4	0.04716	6.1	0.31	21.4	0.9	21.7	2.8	57.5	145.1	1.5
	67	874	627	0.856	0.003308	1.5	0.025652	4.8	0.05623	4.6	0.32	21.3	0.7	25.7	2.4	461.7	101.2	17.2
	68	975	595	0.73	0.003368	1.6	0.023608	4.9	0.05083	4.7	0.33	21.7	0.7	23.7	2.3	233.3	107.8	8.5
	69	716	380	0.635	0.003326	1.8	0.02295	5	0.05004	4.7	0.35	21.4	0.8	23	2.3	197.1	109.3	7.1
	70	805	424	0.63	0.003356	1.8	0.022568	5.6	0.04877	5.3	0.32	21.6	0.8	22.7	2.5	137.1	125.5	4.7
	71	798	457	0.684	0.003441	2.0	0.023712	5.5	0.04998	5.1	0.36	22.1	0.9	23.8	2.6	194	119.5	6.9
	72	3686	7204	2.317	0.003261	1.1	0.021495	3.2	0.04781	3	0.34	21.0	0.4	21.6	1.4	89.7	71.4	2.8
	73	1017	350	0.409	0.003255	1.5	0.023972	5.5	0.05342	5.3	0.27	20.9	0.6	24.1	2.6	346.9	120	12.9
	81	819	422	0.61	0.003325	1.6	0.022004	4.6	0.048	4.3	0.35	21.4	0.7	22.1	2	99.5	102.6	3.2
	82	856	773	1.065	0.003368	1.9	0.03127	4.4	0.06734	4	0.42	21.7	0.8	31.3	2.7	848.3	84	30.7
	83	782	450	0.681	0.003402	1.7	0.023037	3.9	0.04911	3.6	0.42	21.9	0.7	23.1	1.8	153.1	83.5	5.3
	84	1056	709	0.795	0.003329	1.7	0.025121	4.6	0.05473	4.4	0.25	21.4	0.5	25.2	2.3	401.4	99.6	15
	85	912	533	0.691	0.003279	1.2	0.022206	4.6	0.04911	4.3	0.37	21.1	0.7	22.3	2	153.2	100.9	5.4

21.6 ± 0.4 Ma, respectively. From the K-Feldspar megacrystalline granodiorite (KFMG), biotite separates display isochron ages between 21.8 ± 0.1 Ma and 23.2 ± 0.2 Ma. Microgranite-granodiorite (MGG), on the other hand, presents 22.6 ± 0.1 Ma, indicating that two main plutonic members are coeval. K-feldspar and plagioclase separates from the haplogranite displays plateau ages of 20.3 ± 0.2 Ma and 21.6 ± 0.4 Ma, respectively. This shows that, haplogranite, consistent with its field properties, is slightly younger than the main plutonic body.

4.3. Geothermo-barometry Calculations: Al in hornblende geothermo-barometry

Amphibole and plagioclase crystals are widely used by several researchers for pressure and temperature conditions of crystallization

(e.g. Blundy and Holland, 1990; Holland and Blundy, 1994; Anderson and Smith, 1995; Ridolfi et al., 2010; Ridolfi and Renzulli, 2012). The first empirical thermometer was proposed by Blundy and Holland (1990) is based on the reaction between edenite-tremolite for a temperature range between 500 °C and 1100 °C. Afterwards, Holland and Blundy (1994) recalculated the thermometer results based on the edenite-richertite and edenite-tremolite reactions. Both calculations are suitable for calc-alkaline igneous rocks as a result of their stability over a wide P-T range from 400° to 1150 °C and from 1 kbar to 23 kbar (Blundy and Holland, 1990). Several different geobarometry calculations were proposed to determine the emplacement pressure of calc-alkaline felsic plutonic rocks on the basis of Al content in hornblende (Johnson and Rutherford, 1989; Anderson and Smith, 1995; Ridolfi et al., 2010; Ridolfi and Renzulli, 2012). These different pressure and temperature calculations for crystallization conditions are suitable and

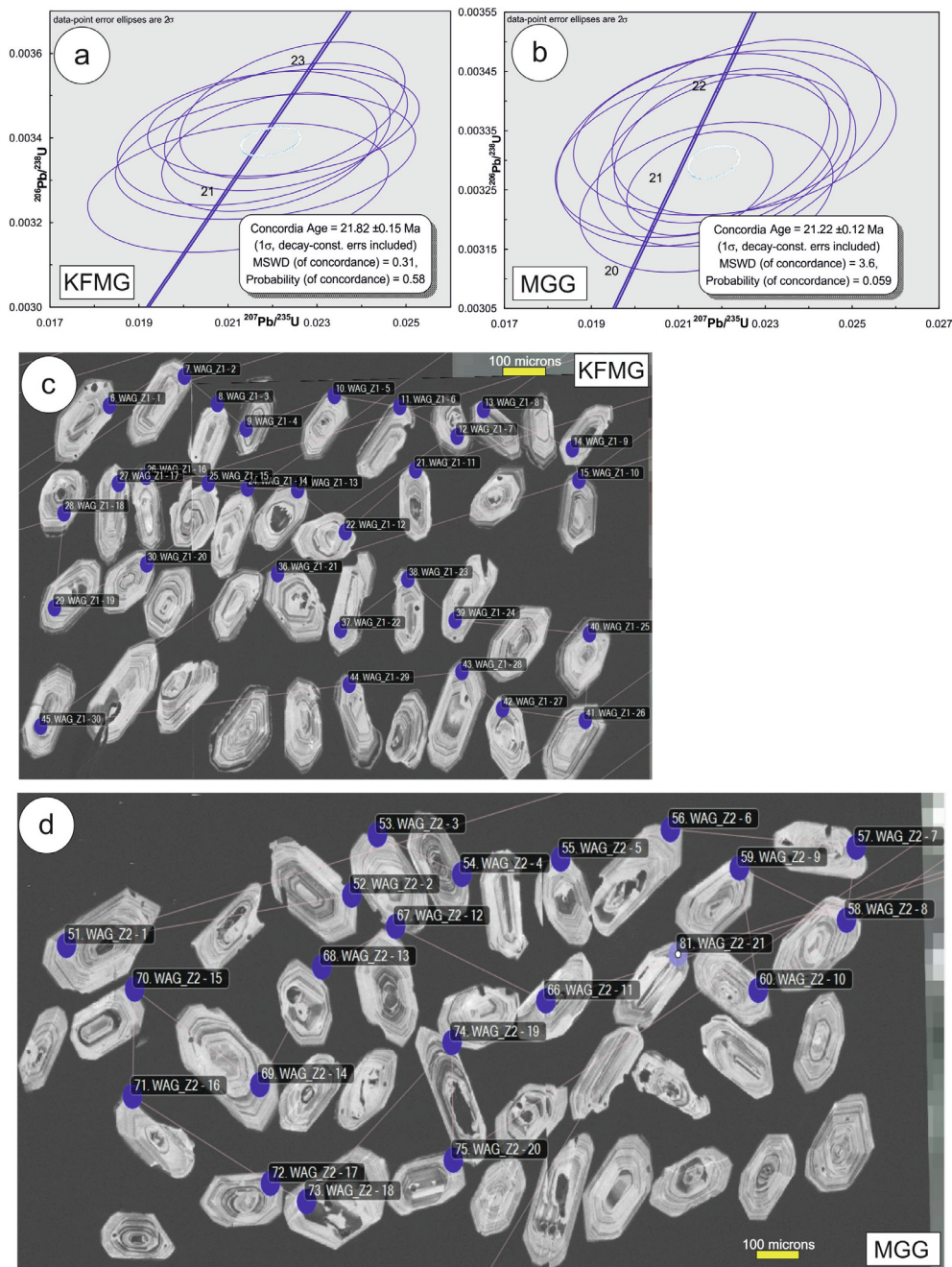


Fig. 10. (a) The $^{206}\text{Pb}/^{238}\text{U}$ vs. $^{207}\text{Pb}/^{235}\text{U}$ concordia diagram for sample AS 211 (KFMG). (b) The $^{206}\text{Pb}/^{238}\text{U}$ vs. $^{207}\text{Pb}/^{235}\text{U}$ concordia diagram for sample AS 240 (MGG). (c) CL images of dated zircon crystals from AS 211 (KFMG). (d) CL images of dated zircon crystals from AS 240 (MGG).

reliable for SP since it is one of the representatives of the felsic calc-alkaline plutonic bodies of western Anatolia (Ünal and Altunkaynak, 2018).

In this study, we analyzed hornblende and plagioclase crystals from nine different samples (six from KFMG and three from MGG) from SP. In total, 89 spots were analyzed from hornblendes and 182 from plagioclases (Supplementary data). Four different calculations were used (Johnson and Rutherford, 1989; Ridolfi et al., 2010; Ridolfi and Renzulli, 2012) to calculate the pressure conditions of the SP. For the temperature conditions, calculations which are proposed by Holland and Blundy (1994), Ridolfi et al. (2010) and Ridolfi and Renzulli (2012) were used. The results of these different calculations are given in Table 3. The results are given both for KFMG and MGG separately for each sample. Table 3 shows that different calculations present different P-T conditions for the emplacement of SP. However, all of the results of

different calculations are reliable based on their stability conditions (400–1150 °C and from 1 kbar to 23 kbar) and chemical properties of the applied rocks (felsic and calc-alkaline plutonic rocks). Therefore, we present the mean results of the P-T calculations of different calculations.

The geothermo-barometry calculations present following results; the mean P and T conditions for different calculations (Johnson and Rutherford, 1989; Holland and Blundy, 1994; Anderson and Smith, 1995; Ridolfi et al., 2010; Ridolfi and Renzulli, 2012) of KFMG are 1.65 kbar and 797 °C, respectively. For MGG, on the other hand, P and T conditions are 0.69 kbar and 745 °C, respectively (Table 3).

5. Discussion: Emplacement of the Solarya pluton

The SP is coeval and cogenetic with hypabyssal and volcanic rocks

Table 2
 $^{40}\text{Ar}/^{39}\text{Ar}$ biotite and feldspar data for the SP. Bi: Biotite; KF: K-feldspar; Plg: Plagioclase.

Sample	Rock Type	Mineral	Integrated Age (Ma)	Weighted Average Age (Ma)	Plateau Information	Isochron Age (Ma)	Isochron or other Information
AS 18	K-Feldspar Megacrystalline granodiorite	Bi	22.4 ± 0.3	22.4 ± 0.3	9 of 10 fractions 99.6% ^{39}Ar release MSWD = 0.49	22.3 ± 0.4	10 of 10 fractions $^{40}\text{Ar}/^{36}\text{Ar}_i = 296.8 \pm 2.7$ MSWD = 0.47
AS 20a	K-Feldspar Megacrystalline granodiorite	Bi	22.9 ± 0.2	23.1 ± 0.2	9 of 10 fractions 99.4% ^{39}Ar release MSWD = 0.99	23.2 ± 0.4	9 of 10 fractions $^{40}\text{Ar}/^{36}\text{Ar}_i = 297.6 \pm 3.3$ MSWD = 1.05
AS 22a	K-Feldspar Megacrystalline granodiorite	Bi	21.7 ± 0.1	21.8 ± 0.1	9 of 10 fractions 99.8% ^{39}Ar release MSWD = 0.19	21.8 ± 0.2	9 of 10 fractions $^{40}\text{Ar}/^{36}\text{Ar}_i = 297.2 \pm 5.9$ MSWD = 0.20
AS 40	Microgranite-granodiorite	Bi	51.6 ± 0.3	22.7 ± 0.2	7 of 10 fractions 96.3% ^{39}Ar release MSWD = 0.67	22.6 ± 0.4	10 of 10 fractions $^{40}\text{Ar}/^{36}\text{Ar}_i = 299.1 \pm 5.0$ MSWD = 0.60
AS 24	Haplogranite	KF	20.6 ± 0.1	20.3 ± 0.4	10 of 13 fractions 69.3% ^{39}Ar release MSWD = 1.44	—	—
AS 24	Haplogranite	Plg	21.9 ± 0.5	21.6 ± 0.8	11 of 13 fractions 97.9% ^{39}Ar release MSWD = 1.00	—	—

(Ünal and Altunkaynak, 2018, 2019 Fig. 12a). The plutons that are spatially and temporally related with cogenetic volcanic rocks are classified as “sub-volcanic plutons” or as “caldera type plutons (Pitcher, 1979; Seager and McCurry, 1988). Therefore, the SP could be classified as “sub-volcanic plutons” or “caldera type plutons” which was emplaced into shallow levels in the crust. However, field relations, petrography and geothermo-barometry studies propose that different members of the SP (KFMG, MGG and haplogranite) were emplaced into different levels of crust through different mechanisms.

KFMG developed a contact metamorphic aureole around it. Contact metamorphism conditions reached to pyroxene-hornfels facies which is commonly observed at the deeper levels of epizone conditions (2 kb/600–750 °C; Musumeci and Vaselli, 2012). The geothermo-barometry calculations reveal that KFMG (the northern part) represents the deeper parts of the pluton and was emplaced around 6–7 km depth (av. 1.65 kbar, 6.1 km depth).

The southern part of the SP is formed from MGG with a distinct fine grained microgranular texture. The contact of MGG and basement rocks are represented by “roof pendant” structure which are generally defined for shallower level intrusions (Fig. 12b). In this contact country rocks are flat and the foliation planes are horizontal. Moreover, the inter-fingering of MGG with the hypabyssal rocks is also a clear indicator for shallow level emplacement (Fig. 12a). This result is also supported by the geothermo-barometer results. Calculated P-T conditions suggest that, MGG was emplaced into the shallower levels with relatively lower pressure conditions (0.69 kbar; 2.4 km). The haplogranite, which is located between KFMG and basement rocks, display graphic/granophytic texture which suggest a shallow, 1.5 km (0.5 kb), emplacement depths (Fig. 12c). Therefore, all these evidences indicate that the KFMG, MGG and haplogranite were emplaced into different depths (between 7 and 1.5 km) of the crust through different emplacement mechanisms.

The emplacement stages of the SP can be summarized into two distinct events; (1) emplacement at the deeper levels of the crust with high temperature (Fig. 13a) and (2) emplacement into shallower levels with relatively lower temperatures (Fig. 13c). The evidences for these stages are summarized as follows;

The emplacement of the SP caused several structural and compositional effects on the country rocks through the eastern and northern contacts. Along the contacts between SP and calc-schists, contact metamorphic rocks are made up of contact schists with the elongation of contact metamorphic minerals such as diopside and wollastonite over a

secondary foliation plane (S-2) with a shear sense pointing outwards the contacts of the pluton. Development of contact schists with these types of structural properties are commonly attributed to the forceful emplacement of the plutonic bodies (Sardinha et al., 2006; Stevenson, 2009; Festa et al., 2013). Moreover, the foliation planes of the wall rocks progressively swing towards to the pluton boundary. At these boundaries the positions of the wall contacts are steeply dipping outwards the pluton contacts. Stevenson et al. (2007) proposed that, steeply dipping contacts are due to the upward directed forces from a forceful emplacement (Fig. 13a).

After this stage, even if the KFMG was emplaced and consolidated, the pluton is not completely fulfilled its emplacement and there is still magma left (Read, 1957) evidenced by the overlapping emplacement age of MGG with the intrusion of hypabyssal rocks and accumulation of a thick volcanic sequence. This is shown by the radiometric age results of plutonic, hypabyssal and volcanic rocks which are coeval (Ünal and Altunkaynak, 2019). The spatial and temporal connection of plutonic (MGG and KFMG), hypabyssal and volcanic rocks may suggest that the whole magmatic complex has passed through a caldera collapse environment and therefore the static elevation of MGG could be provided by cauldron subsidence mechanism evidenced by as follows.

The forceful emplacement of the SP into the brittle zone of the crust causes to the development of ring and radial fractures in the country rocks around the main plutonic body (Fig. 13b). Hypabyssal rocks (sheet intrusives) were emplaced into these fractures almost coevally with the pluton. Not only the sheet intrusive rocks, but also the main plutonic body (MGG) was elevated into the shallower levels with the aid of these fractures and faults. The MGG which represents the roof of the plutonic body as a shallower part of the SP is located at the southern part of the main body. Topographically, this southern part is represented by shallower elevations. Under normal circumstances, the shallower parts are expected to be located at the topographically upper parts of the pluton. However, the MGG is well preserved even at the lower elevations which may have been emplaced with the block subsidence along ring fractures/faults. Indeed, the current topography of the region may have been shaped by erosion and young structural features but these types of topographical patterns are commonly defined as a possible evidence for granite emplacement by cauldron subsidence mechanism similar to Pearly Gates Pluton (Myers et al., 2008), Mount Lister Pluton (Myers et al., 2008) and Kozak Pluton (Altunkaynak and Yılmaz, 1999). The subsidence of blocks resulted in a decompression of the volume which must have been filled with MGG

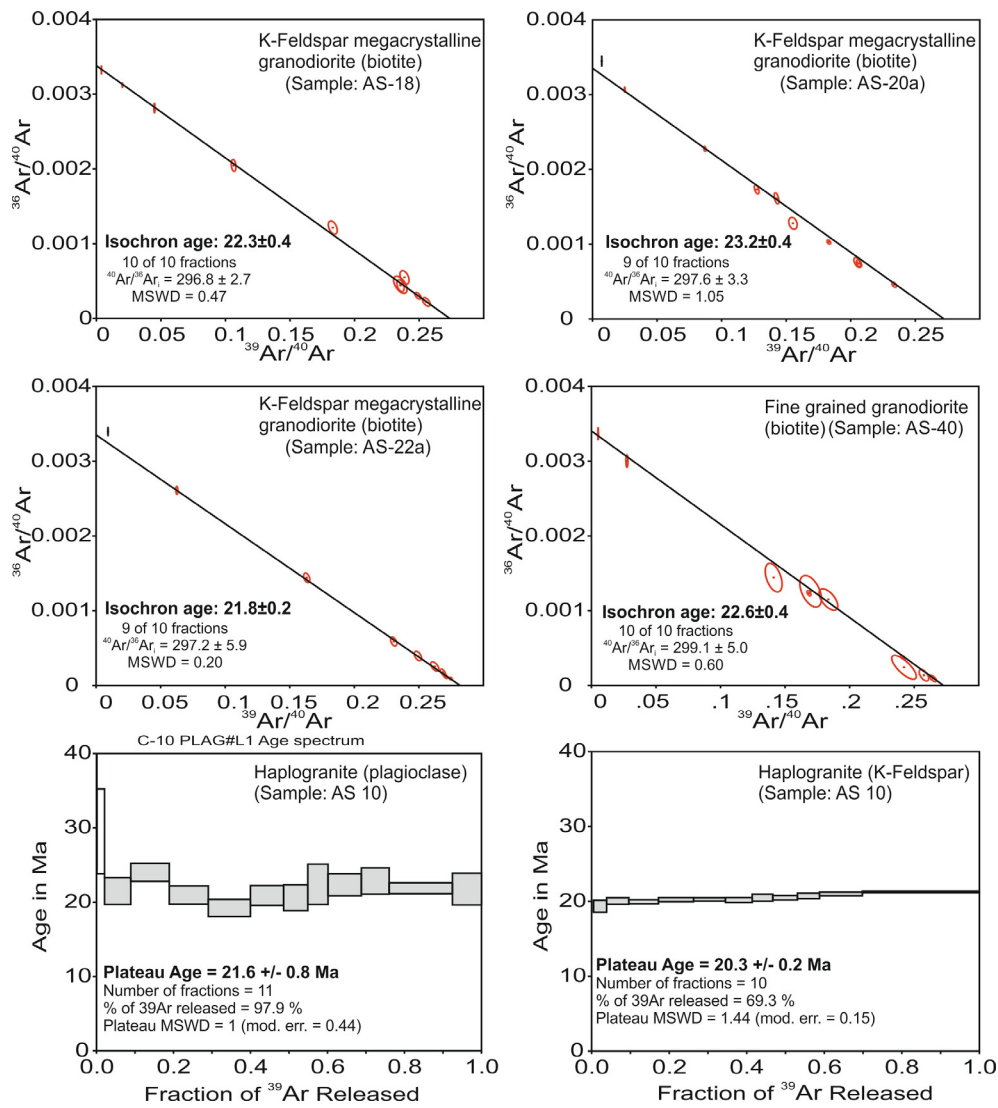


Fig. 11. $^{40}\text{Ar}/^{39}\text{Ar}$ isochron and plateau ages of the SP. The sample name and group are shown on each of the diagrams. Steps in red are used in the isochron age determinations. Steps in grey are used in the plateau age determinations. (For interpretation of the references to colour in this figure legend, the reader is referred to the web version of this article.)

Table 3
Amphibole-plagioclase geothermo-barometry results for the SP.

Reference	Unit	K-Feldspar Megacrystalline Granodiorite (KFMG)					Microgranite-granodiorite (MGG)				
		AS16	AS22a	AS16a	AS81	AS9	AS13	AS120	AS115	AS113	
Ridolfi et al. (2010)	T (°C)	851.11	837.43	827.79	831.38	830.08	855.27	762.02	796.40	775.40	
Ridolfi and Renzulli (2012)	T (°C)	786.96	739.89	792.12	807.86	799.36	803.23	719.88	631.07	685.38	
Holand and Blundy (1994)	T (°C)	819.08	776.30	808.98	818.21	834.84	844.09	758.64	800.07	804.12	
Holand and Blundy (1994)	T (°C)	768.62	716.18	737.29	698.94	772.03	777.16	736.75	723.21	751.25	
Average	T (°C)	797.26						745.35			
Ridolfi et al. (2010)	P (kbar)	1.37	1.24	1.14	1.15	1.33	1.55	0.70	0.53	0.52	
Ridolfi and Renzulli (2012)	P (kbar)	1.28	1.03	1.20	1.29	1.40	1.50	0.68	0.42	0.48	
Anderson and Smith (1995)	P (kbar)	1.92	1.80	1.90	1.95	1.86	1.99	1.10	1.68	0.72	
Johnson and Rutherford (1989)	P (kbar)	2.30	2.00	1.67	1.77	2.20	2.67	0.78	0.39	0.14	
Average	P (kbar)	1.65						0.69			
Ridolfi et al. (2010)	Depth (km)	5.06	4.58	4.21	4.25	4.91	5.72	2.58	1.97	1.92	
Ridolfi and Renzulli (2012)	Depth (km)	4.74	3.82	4.43	4.76	5.16	5.54	2.53	1.55	1.77	
Anderson and Smith (1995)	Depth (km)	7.10	6.88	7.03	7.21	6.88	7.36	4.07	6.22	2.16	
Johnson and Rutherford (1989)	Depth (km)	8.52	7.39	6.19	6.56	8.12	9.88	2.87	1.14	0.52	
Average	Depth (km)	6.1						2.44			

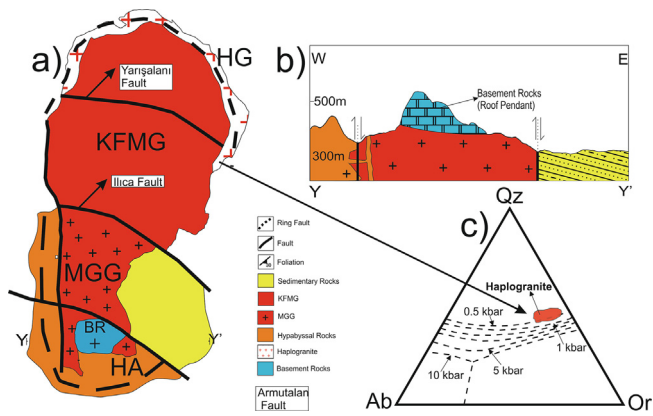


Fig. 12. (a) Ring fractures/faults developed due to the emplacement of the SP. Haplogranite and hypabyssal association were emplaced into the ring faults, which are shown by dashed lines. (b) W-E cross section along the southern contact of the SP (horizontally not to scale, the cross-section directions are shown in Fig. 12a). (c) Qz-Ab-Or triangle illustrating the pressure conditions of haplogranites (Tuttle and Bowen, 1958).

the central part of the SP but also developed along the contacts of the SP with country rocks. The existence of arch-shaped outcrops of sheet intrusives (cone sheets) which surround and dip outwards the pluton indicate that magma was probably elevated to shallower levels in the crust with the aid of ring fractures. Through these fractures, haplogranites were emplaced (Fig. 13c). The emplacement of the haplogranite must have occurred at shallower levels as evidenced by graphic/granophytic textures (Tuttle and Bowen, 1958). Therefore, the successive development of cauldron subsidence mechanism after the forceful emplacement could provide the permissive emplacement of the pluton to the sub-volcanic levels in the crust as a result of the sinking of a large country rock block facilitated by fractures or faults into a magma chamber which is replaced by magma from the same chamber (Fig. 13c). Cauldron subsidence is fundamentally the subterranean or plutonic version of caldera collapse (Clough et al., 1909; Richey, 1932; Anderson, 1936; Hills, 1963; Hall, 1996; Cole et al., 2005).

Richey (1928) proposed a model for the emplacement of the remaining magma into the space created by the block subsidence. This model suggests that, the emplacement of new magma occurs through repetitive stages. We adapted this model to the SP with combining our field, structural, geothermo-barometry and geochronology data (Fig. 14). The model proposes that, the upwelling of new magma initiated with the emplacement of microgranite-granodiorite (MGG) which is geochemically and isotopically identical to KFMG (Ünal and Altunkaynak, 2018, 2019). This is followed by the emplacement of the sheet intrusives. The haplogranites were emplaced into the ring faults/fractures at the final stage. The model proposes that, these magmas gradually pass into each other which is consistent with our field observations. This sequence of the new magma emplacement is also evidenced by the $^{40}\text{Ar}/^{39}\text{Ar}$ dating of the MGG, hypabyssal rocks and haplogranites. The MGG presents a 22.8 Ma $^{40}\text{Ar}/^{39}\text{Ar}$ age and hypabyssal rocks display $^{40}\text{Ar}/^{39}\text{Ar}$ age of 22.5 Ma (Ünal and Altunkaynak, 2019). Haplogranites, on the other hand, yielded a $^{40}\text{Ar}/^{39}\text{Ar}$ age of 20.6 Ma, representing the youngest member of the SP.

There is almost a total consensus that the early Miocene magmatic rocks along northwestern Anatolia formed under an extensional tectonic regime (or syn-convergent extension; (Altunkaynak and Dilek, 2006; Boztuğ et al., 2009; Erkül, 2009; Öner et al., 2010; Altunkaynak et al., 2012; Ünal and Altunkaynak, 2018). The geology and petrogenesis of the SP, as presented in detail by Altunkaynak et al., 2012; Ünal and Altunkaynak, 2018, 2019 indicate clearly that the pluton was emplaced during the period when the region was suffering N-S extension. The subsequent forceful to passive (cauldron subsidence) emplacement and shallow nature of the SP also support this result. Cauldron subsidence mechanism (and passive emplacement) developed extensively under extensional regime exemplified by many plutonic and volcano-plutonic complexes such as Rosses Granitic Complex, Ireland

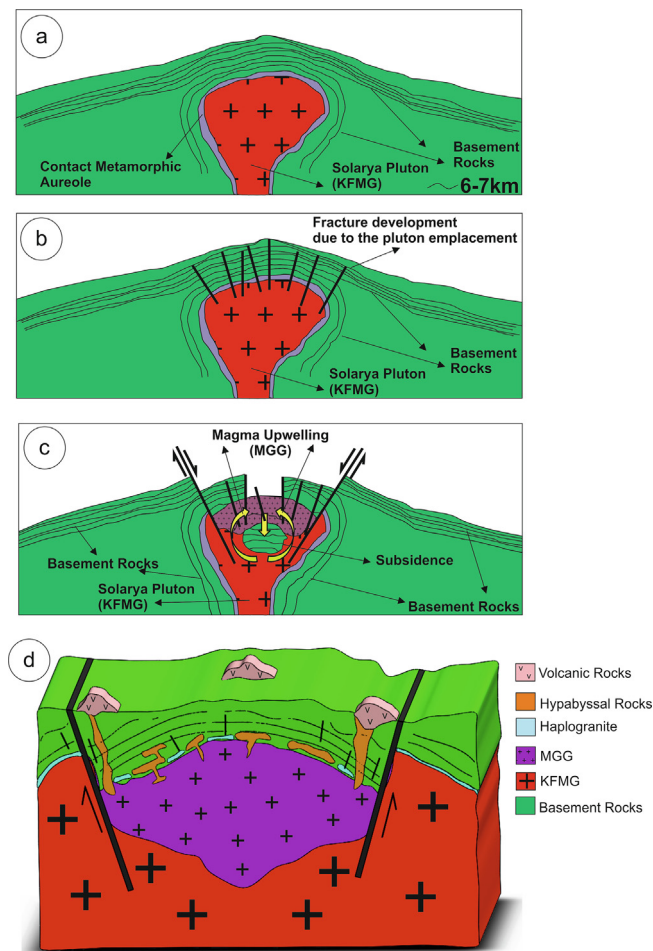


Fig. 13. Schematic cross-sections illustrating the consecutive emplacement stages of the SP. (a) The forceful emplacement of the SP. (b) Fracture development due to the pluton emplacement. (c) Passive emplacement (cauldron subsidence) stage of the SP d) Block diagram showing the final position of the SP.

magma. In the latter stages, these faults were re-activated and formed the topographical difference between KFMG and MGG.

The subsidence was not only occurred along the ring faults through

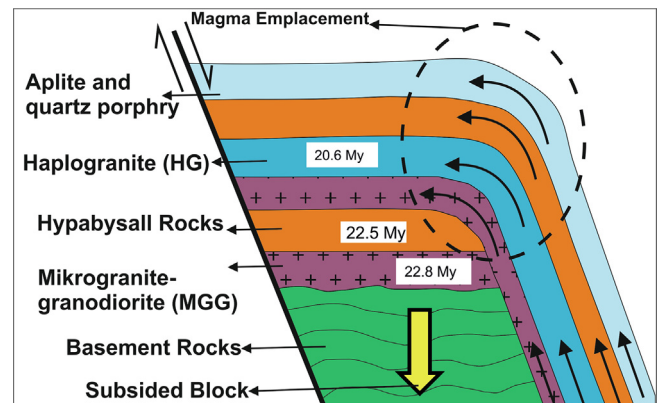


Fig. 14. Schematic diagram of the upwelling magma in cauldron subsidence (adapted from Richey, 1928).

(Stevenson, 2009), Wiborg and Åland Granites, Finland (Karell et al., 2014) and Štiavnica Volcano-plutonic Complex, Western Carpathians (Tomek et al., 2014).

6. Conclusions

- The SP consists of three main plutonic members showing different textural properties; a northern part of the plutonic body is represented by K-feldspar megacrystalline granodiorite (KFMG) with distinct porphyritic texture and southern part is made up of microgranite-granodiorite (MGG) displaying microgranular texture whereas haplogranite, which displays graphic/granophytic textures, is represented by a thin aureole between the SP and basement rocks.
- The $^{40}\text{Ar}/^{39}\text{Ar}$ biotite ages for KFMG yield between 21.8 ± 0.1 Ma and 23.2 ± 0.2 Ma. For MGG, $^{40}\text{Ar}/^{39}\text{Ar}$ biotite age is 22.6 ± 0.1 Ma, indicating that two main plutonic members are coeval. K-feldspar and plagioclase separates from the haplogranite display plateau ages of 20.3 ± 0.2 Ma and 21.6 ± 0.4 Ma, respectively.
- The U-Pb zircon ages obtained from KFMG and MGG are 21.8 ± 0.2 and 21.2 ± 0.1 Ma, respectively.
- KFMG have 1.65 kbar pressure and 797 °C temperature emplacement conditions. For MGG, on the other hand, P and T conditions are 0.69 kbar and 745 °C, respectively.
- The SP were emplaced into different levels of crust with different mechanisms. The SP began its emplacement forcefully in relatively deeper levels in the crust (6.1 km depth). After this stage, MGG was emplaced into the shallow levels (2.4 km depth) via cauldron subsidence and in the late stage the sheet intrusive rocks were emplaced into the ring faults at 1.5 km depth.
- The forceful to passive emplacement of the SP occurred under Aegean extensional tectonics during the Miocene.

Declaration of Competing Interest

The authors declare that they have no known competing financial interests or personal relationships that could have appeared to influence the work reported in this paper.

Acknowledgment

This article is a part of Alp Ünal's doctoral dissertation work and has been supported by grants from TUBITAK (CAYDAG- 112Y093) to ŞA. The authors are grateful to Chris Fleisher for his help on microprobe studies. We would like to thank two anonymous reviewers and Dr. İbrahim Uysal for their useful comments.

Appendix A. Supplementary material

Supplementary data to this article can be found online at <https://doi.org/10.1016/j.jseaes.2019.103979>.

References

Altunkaynak, Ş., 2007. Collision-driven slab breakoff magmatism in northwestern Anatolia, Turkey. *J. Geol.* 115 (1), 63–82.

Altunkaynak, Ş., Dilek, Y., Genç, S.C., Sunal, G., Gertisser, R., Furnes, H., Foland, K.A., Yang, J., 2012. Spatial, temporal and geochemical evolution of Oligo-Miocene granitoid magmatism western Anatolia, Turkey. *Gondwana Res.* 21, 961–986.

Altunkaynak, Ş., Yılmaz, Y., 1999. The Kozak Pluton and its emplacement. *Geol. J.* 34 (3), 257–274.

Altunkaynak, Ş., Rogers, N.W., Kelley, S.P., 2010. Causes and effects of geochemical variations in late Cenozoic volcanism of the Foça volcanic centre, NW Anatolia, Turkey. *Int. Geol. Rev.* 52 (4–6), 579–607.

Altunkaynak, Ş., Dilek, Y., 2006. Timing and nature of postcollisional volcanism in western Anatolia and geodynamic implications. *SPECIAL PAPERS-GEOLOGICAL SOCIETY OF AMERICA* 321–349.

Anderson, E.M., 1936. The dynamics of the formation of cone-sheets, ring-dykes, and cauldron-subsidences. *Proc. Roy. Soc. Edinb.* 56 (2), 128–163.

Anderson, J.L., Smith, D.R., 1995. The effect of temperatures and oxygen fugacity on Al-in-hornblende barometry. *Am. Mineral.* 87, 125–138.

Armstrong, R.L., Clark, S.P., 1988. Mesozoic and early Cenozoic magmatic evolution of the Canadian Cordillera. *Geol. Soc. Am. Spec. Pap.* 218, 55–91.

Benowitz, J.A., Layer, P.W., Vanlaningham, S., 2014. Persistent long-term (c. 24 Ma) exhumation in the Eastern Alaska Range constrained by stacked thermochronology. *Geol. Soc. Lond. Special Publ.* 378 (1), 225–243.

Blundy, J.D., Holland, T.J., 1990. Calcic amphibole equilibria and a new amphibole-plagioclase geothermometer. *Contrib. Miner. Petrol.* 104 (2), 208–224.

Boztuğ, D., Harlavan, Y., Jonckheere, R., Can, İ., Sari, R., 2009. Geochemistry and K-Ar cooling ages of the Ilca, Çataldağ (Balıkesir) and Kozak (İzmir) granitoids, west Anatolia, Turkey. *Geol. J.* 44 (1), 79–103.

Brown, M., 1994. The generation, segregation, ascent and emplacement of granite magma: the migmatite-to-crustally-derived granite connection in thickened orogens. *Earth Sci. Rev.* 36 (1–2), 83–130.

Clemens, J.D., 1998. Observations on the origins and ascent mechanisms of granitic magmas. *Journal of the Geological Society* 155 (5), 843–851.

Clough, C.T., Maufe, H.B., Bailey, E.B., 1909. The cauldron-subsidence of Glen Coe, and the associated igneous phenomena. *Quart. J. Geol. Soc.* 65 (1–4), 611–678.

Cole, J.W., Milner, D.M., Spinks, K.D., 2005. Calderas and caldera structures: a review. *Earth Sci. Rev.* 69 (1–2), 1–26.

Cruden, A.R., 1998. On the emplacement of tabular granites. *J. Geol. Soc.-Lond.* 155 (5), 853–862.

Çelebi, D., Köprübaşı, N., 2014. The geochemical and Sr–Nd isotopic characteristics of Eocene to Miocene NW Anatolian granitoids: Implications for magma evolution in a post-collisional setting. *J. Asian Earth Sci.* 93, 275–287.

Dunkl, I., Mikes, T., Simon, K., von Eynatten, H., 2008. Brief introduction to the Windows program *Pepita*: data visualization, and reduction, outlier rejection, calculation of trace element ratios and concentrations from LA-ICP-MS data. In: Sylvester, P. (Ed.), *Laser Ablation ICP-MS in the Earth Sciences: Current Practices and Outstanding Issues*. Mineralogical Association of Canada, Short Course, pp. 334–340.

Emre, Ö., Duman, T.Y., Özalp, S., Şaroğlu, F., Olgun, Ş., Elmacı, H., Çan, T., 2018. Active fault database of Turkey. *Bull. Earthq. Eng.* 16 (8), 3229–3275.

Erkül, F., 2009. Tectonic significance of synextensional ductile shear zones within the Early Miocene Alaçamdağ granites, northwestern Turkey. *Geol. Mag.* 147 (4), 611–637.

Erkül, S.T., 2012. Petrogenetic evolution of the Early Miocene Alaçamdağ volcano-plutonic complex, northwestern Turkey: implications for the geodynamic framework of the Aegean region. *Int. J. Earth Sci.* 101 (1), 197–219.

Festa, V., Caggianelli, A., Langone, A., Prosser, G., 2013. Time–space relationships among structural and metamorphic aureoles related to granite emplacement: a case study from the Serre Massif (southern Italy). *Geol. Mag.* 150 (3), 441–454.

Frei, D., Gerdes, A., 2009. Precise and accurate in situ U–Pb dating of zircon with high sample throughput by automated LA-SF-ICP-MS. *Chem. Geol.* 261 (3–4), 261–270.

Genç, S.C., Yılmaz, Y., 1997. An example of post-collisional magmatism in northwestern Anatolia: the Kızderbent volcanics (Armutlu peninsula, Turkey). *Turk. J. Earth Sci.* 6 (1), 33–42.

Hall, A., Pereira, M.D., Bea, F., 1996. The abundance of ammonium in the granites of central Spain, and the behaviour of the ammonium ion during anatexis and fractional crystallization. *Mineral. Petrol.* 56 (1–2), 105–123.

Helvacı, C., Ersoy, Y.E., Sözbilir, H., Erkül, F., Sümer, Ö., Uzel, B., 2009. Geochemistry and $^{40}\text{Ar}/^{39}\text{Ar}$ geochronology of Miocene volcanic rocks from the Karaburun Peninsula: implications for amphibole-bearing lithospheric mantle source, Western Anatolia. *J. Volcanol. Geotherm. Res.* 185 (3), 181–202.

Hills, S.E., 1963. *Elements of Structural Geology*. Wiley, New York.

Holland, T., Blundy, J., 1994. Non-ideal interactions in calcic amphiboles and their bearing on amphibole-plagioclase thermometry. *Contrib. Miner. Petrol.* 116 (4), 433–447.

Hutton, D.H., 1988. Granite emplacement mechanisms and tectonic controls: inferences from deformation studies. *Earth Environ. Sci. Trans. R. Soc. Edinburgh* 79 (2–3), 245–255.

Jackson, S.E., Pearson, N.J., Griffin, W.L., Belousova, E.A., 2004. The application of laser ablation-inductively coupled plasma-mass spectrometry to in situ U–Pb zircon geochronology. *Chem. Geol.* 211 (1–2), 47–69.

Johnson, M.C., Rutherford, M.J., 1989. Experimental calibration of the aluminum-in-hornblende geobarometer with application to Long Valley caldera (California) volcanic rocks. *Geology* 17 (9), 837–841.

Kamacı, Ö., Altunkaynak, Ş., 2019. Cooling and deformation history of the Çataldağ Metamorphic Core Complex (NW Turkey). *J. Asian Earth Sci.* 172, 279–291.

Kamacı, Ö., Altunkaynak, Ş., 2019. Magma chamber processes and dynamics beneath northwestern Anatolia: Insights from mineral chemistry and crystal size distributions (CSDs) of the Kepsut Volcanic Complex (NW Turkey). *J. Asian Earth Sci.* 181.

Karacık, Z., Yılmaz, Y., Pearce, J.A., Ece, Ö.I., 2008. Petrochemistry of the south Marmara granitoids, northwest Anatolia, Turkey. *Int. J. Earth Sci.* 97 (6), 1181–1200.

Karell, F., Ehlers, C., Airo, M.L., 2014. Emplacement and magnetic fabrics of rapakivi granite intrusions within Wiborg and Åland rapakivi granite batholiths in Finland. *Tectonophysics* 614, 31–43.

Layer, P.W., Hall, C.M., York, D., 1987. The derivation of $^{40}\text{Ar}/^{39}\text{Ar}$ age spectra of single grains of hornblende and biotite by laser step-heating. *Geophys. Res. Lett.* 14 (7), 757–760.

Ludwig, K., 2003. *Isoplot/Ex 3.0. A Geochronological Toolkit for Microsoft Excel*. Berkeley Geochronology Center, Berkeley, CA, USA Special Publication, (4).

Marsh, B.D., 1982. On the mechanics of igneous diapirism, stoping, and zone melting. *Am. J. Sci.* 282 (6), 808–855.

McCaffrey, K.J.W., Petford, N., 1997. Are granitic intrusions scale invariant? *J. Geol. Soc.* 154 (1), 1–4.

- McDougall, I., Mac Dougall, I., Harrison, T.M., 1999. Geochronology and Thermochronology by the $^{40}\text{Ar}/^{39}\text{Ar}$ Method. Oxford University Press on Demand.
- Musumeci, G., Vaselli, L., 2012. Neogene deformation and granite emplacement in the metamorphic units of northern Apennines (Italy): Insights from mylonitic marbles in the Porto Azzurro pluton contact aureole (Elba Island). *Geosphere* 8 (2), 470–490.
- Myers, J.S., Voordouw, R.J., Tettelaar, T.A., 2008. Proterozoic anorthosite–granite Nain batholith: structure and intrusion processes in an active lithosphere-scale fault zone, northern Labrador. *Canadian Journal of Earth Sciences* 45 (8), 909–934.
- Okay, A.I., 1984. Distribution and characteristics of the north-west Turkish blueschists. *Geol. Soc. Lond. Special Publ.* 17 (1), 455–466.
- Okay, A.I., Siyako, M., Bürkan, K.A., 1990. Geology and tectonic evolution of the Biga Peninsula (in Turkish). *Bull. Turk. Assoc. Petrol. Geol.* 2, 83–121.
- Öner, Z., Dilek, Y., Kadioğlu, Y.K., 2010. Geology and geochemistry of the synextensional Salihli granitoid in the Menderes core complex, western Anatolia, Turkey. *International Geology Review* 52 (2–3), 336–368.
- Paces, J.B., Miller Jr., J.D., 1993. Precise U–Pb ages of Duluth complex and related mafic intrusions, northeastern Minnesota: Geochronological insights to physical, petrogenetic, paleomagnetic, and tectonomagmatic processes associated with the 1.1 Ga midcontinent rift system. *J. Geophys. Res. Solid Earth* 98 (B8), 13997–14013.
- Paterson, S.R., Fowler Jr., T.K., 1993. Re-examining pluton emplacement processes. *J. Struct. Geol.* 15 (2), 191–206.
- Petford, N., Cruden, A.R., McCaffrey, K.J.W., Vigneresse, J.L., 2000. Granite magma formation, transport and emplacement in the Earth's crust. *Nature* 408 (6813), 669.
- Pitcher, W.S., 1979. The nature, ascent and emplacement of granitic magmas. *J. Geol. Soc.* 136 (6), 627–662.
- Pitcher, W.S., 1993. The nature and origin of granites. Blackie Academic & Professional, London, pp. 1–321.
- Read, H.H., 1957. The Granite Controversy. Murby, London.
- Renne, P.R., Deino, A.L., Walter, R.C., Turrin, B.D., Swisher III, C.C., Becker, T.A., Curtis, G.H., Sharp, W.D., Jaouni, A.R., 1994. Intercalibration of astronomical and radio-isotopic time. *Geology* 22 (9), 783–786.
- Renne, P.R., Mundil, R., Balco, G., Min, K., Ludwig, K.R., 2010. Joint determination of 40K decay constants and $^{40}\text{Ar}/^{40}\text{K}$ for the Fish Canyon sanidine standard, and improved accuracy for $^{40}\text{Ar}/^{39}\text{Ar}$ geochronology. *Geochimica et Cosmochimica Acta* 74 (18), 5349–5367.
- Richey, J.E., 1928. The structural relations of the Mourne granites, Northern Ireland. *Quart. J. Geol. Soc.* 83 (1–5), 653–NP.
- Richey, J.E., 1932. The tertiary ring complex of Slieve Gullion (Ireland), with petrological notes by Herbert Henry Thomas. *Quart. J. Geol. Soc.* 88 (1–4), 776–849.
- Ridolfi, F., Renzulli, A., 2012. Calcic amphiboles in calc-alkaline and alkaline magmas: thermobarometric and chemometric empirical equations valid up to 1,130° C and 2.2 GPa. *Contrib. Miner. Petrol.* 163 (5), 877–895.
- Ridolfi, F., Renzulli, A., Puerini, M., 2010. Stability and chemical equilibrium of amphibole in calc-alkaline magmas: an overview, new thermobarometric formulations and application to subduction-related volcanoes. *Contrib. Miner. Petrol.* 160 (1), 45–66.
- Samson, S.D., Alexander Jr, E.C., 1987. Calibration of the interlaboratory $^{40}\text{Ar}/^{39}\text{Ar}$ dating standard, MMhb-1. *Chem. Geol.: Isotope Geosci. Sect.* 66 (1–2), 27–34.
- Sardinha, A.S., de Mesquita Barros, C.E., Krymsky, R., 2006. Geology, geochemistry, and U–Pb geochronology of the Archean (2.74 Ga) Serra do Rabo granite stocks, Carajás Metallogenic Province, northern Brazil. *J. S. Am. Earth Sci.* 20 (4), 327–339.
- Seager, W.R., McCurry, M., 1988. The cogenetic organ cauldron and batholith, south central New Mexico: Evolution of a large-volume ash flow cauldron and its source magma chamber. *J. Geophys. Res. Solid Earth* 93 (B5), 4421–4433.
- Sircombe, K.N., Hazelton, M.L., 2004. Comparison of detrital zircon age distributions by kernel functional estimation. *Sed. Geol.* 171 (1–4), 91–111.
- Sláma, J., Košler, J., Condon, D.J., Crowley, J.L., Gerdes, A., Hanchar, J.M., Horstwood, M.S.A., Morris, G.A., Nasdala, L., Norberg, N., Schaltegger, U., Schoene, B., Tubrett, M.N., Whitehouse, M.J., 2008. Plešovice zircon—a new natural reference material for U–Pb and Hf isotopic microanalysis. *Chem. Geol.* 249 (1–2), 1–35.
- Stevenson, C., 2009. The relationship between forceful and passive emplacement: The interplay between tectonic strain and magma supply in the Rosses Granitic Complex, NW Ireland. *J. Struct. Geol.* 31 (3), 270–287.
- Stevenson, C.T., Owens, W.H., Hutton, D.H., 2007. Flow lobes in granite: The determination of magma flow direction in the Travenagh Bay Granite, northwestern Ireland, using anisotropy of magnetic susceptibility. *Geol. Soc. Am. Bull.* 119 (11–12), 1368–1386.
- Stevenson, C., Hutton, D., Price, A., 2008. The Travenagh Bay Granite and a new model for the emplacement of the Donegal Batholith. *Trans. R. Soc. Edinburgh: Earth Sci.* 97 (4), 455–477.
- Tomek, F., Žák, J., Holub, F.V., Chlupáčová, M., Verner, K., 2014. Growth of intra-caldera lava domes controlled by various modes of caldera collapse, the Štiavnica volcano–plutonic complex, Western Carpathians. *Journal of Volcanology and Geothermal Research* 311, 183–197.
- Tuttle, O.F., Bowen, N.L., 1958. Origin of granite in the light of experimental studies in the system $\text{NaAlSi}_3\text{O}_8\text{--KAlSi}_3\text{O}_8\text{--SiO}_2\text{--H}_2\text{O}$. *Geol. Soc. Am.*
- Şengör, A.M.C., Yılmaz, Y., 1981. Tethyan evolution of Turkey: a plate tectonic Approach. *Tectonophysics* 75, 181–241.
- Ünal, A., Altunkaynak, Ş., 2018. Nature and genesis of potassic high BaSr granitoids associated with syn-convergent extension in NW Turkey. *Lithos* 316, 261–277.
- Ünal, A., Altunkaynak, Ş., 2019. Interplay between volcanic and plutonic systems: A case study of the early Miocene Solarya Volcano-plutonic Complex in NW Anatolia (Turkey). *J. Asian Earth Sci.* 179, 319–336.
- Wiedenbeck, M.A.P.C., Alle, P., Corfu, F., Griffin, W.L., Meier, M., Oberli, F.V., Quadt, A.V., Roddick, J.C., Spiegel, W., 1995. Three natural zircon standards for U–Th–Pb, Lu–Hf, trace element and REE analyses. *Geostand. Newsl.* 19 (1), 1–23.
- Yardley, B.W.D., McKenzie, W.S., Guilford, C., 1990. Atlas of Metamorphic Rocks and Their Textures. Longman Scientific and Technical, Essex.
- Yılmaz, E., Güleç, N., Kuşcu, İ., Lentz, D.R., 2014. Geology, geochemistry, and geochronology of Fe-oxide Cu (\pm Au) mineralization associated with Şamlı pluton, western Turkey. *Ore Geol. Rev.* 57, 191–215.